PHYSICAL REVIEW D **93,** 114516 (2016)

Interpreting numerical measurements in fixed topological sectors

Wolfgang Bietenholz,[1] Christopher Czaban,[2] Arthur Dromard,[2] Urs Gerber,[1,3] Christoph P. Hofmann,[4] Héctor Mejía-Díaz,[1] and Marc Wagner[2]

[1]*Instituto de Ciencias Nucleares, Universidad Nacional Autónoma de México, A.P. 70-543, C.P. 04510 Ciudad de México, Mexico*

[2]*Institut für Theoretische Physik, Goethe-Universität Frankfurt am Main, Max-von-Laue-Straße 1, D-60438 Frankfurt am Main, Germany*

[3]*Instituto de Física y Matemáticas, Universidad Michoacana de San Nicolás de Hidalgo, Edificio C-3, Apdo. Postal 2-82, C.P. 58040, Morelia, Michoacán, Mexico*

[4]*Facultad de Ciencias, Universidad de Colima, Bernal Díaz del Castillo 340, Colima C.P. 28045, Mexico*

(Received 27 April 2016; published 28 June 2016)

For quantum field theories with topological sectors, Monte Carlo simulations on fine lattices tend to be obstructed by an extremely long autocorrelation time with respect to the topological charge. Then reliable numerical measurements are feasible only within individual sectors. The challenge is to assemble such restricted measurements in a way that leads to a substantiated approximation to the fully fledged result, which corresponds to the correct sampling over the entire set of configurations. We test an approach for such a topological summation, which was suggested by Brower, Chandrasekharan, Negele and Wiese. Under suitable conditions, energy levels and susceptibilities can be obtained to a good accuracy, as we demonstrate for O(N) models, SU(2) Yang-Mills theory, and for the Schwinger model.

DOI: 10.1103/PhysRevD.93.114516

I. MOTIVATION

We consider quantum field theories with topological sectors, in Euclidean spacetime. These sectors are characterized by a topological charge $Q \in \mathbb{Z}$, which is a functional of the field configuration. In infinite volume, the configurations with finite action are divided into these disjoint sectors. The same property holds in finite volume with periodic boundary conditions.

Examples are O(N) models in $d = N - 1$ dimensions, all two-dimensional $CP(N-1)$ models, four-dimensional SU(N) Yang-Mills gauge theories ($N \geq 2$), as well as QCD, and two-dimensional U(1) gauge theory, as well as the Schwinger model. In all these models, a continuous deformation of a given configuration (at finite action) can only lead to configurations within the same topological sector, i.e., the deformation cannot alter the topological charge Q.

In light of this definition, lattice regularized models have in general no topological sectors—strictly speaking. Nevertheless, it is often useful to divide the set of lattice field configurations into sectors, which turn into the topological sectors in the continuum limit. The definition of a topological charge on the lattice is somewhat arbitrary. In the presence of chiral fermions (where the lattice Dirac operator obeys the Ginsparg-Wilson relation), the fermion index provides a sound formulation [1]. For the O(N) models the geometric definition [2] is optimal, since it guarantees integer topological charges on periodic lattices (for all configurations except for a subset of measure 0). In gauge theory, field theoretic definitions are often applied, usually combined with smearing or cooling techniques; see, e.g., Ref. [3]. These techniques are computationally cheap and provide, on fine lattices or at fixed topology, results which agree well with the computationally demanding fermion index [4–6].

As we proceed to finer and finer lattices, the formulation becomes more continuumlike, and changing a (suitably defined) topological sector of the lattice field gets more and more tedious—for this purpose, continuous deformations have to pass through a statistically suppressed domain of high Euclidean action. To a large extent, this property persists for finite but small deformations, as they are carried out in the Markov chain of a Monte Carlo simulation which performs small update steps.

In QCD simulations with dynamical quarks, the gauge configurations are usually generated with a Hybrid Monte Carlo (HMC) algorithm, with small updates, on lattices of a spacing a in the range $0.05\ \mathrm{fm} \lesssim a \lesssim 0.15\ \mathrm{fm}$. The artifacts due to the finite lattice spacing tend to be the main source of systematic errors. Therefore, the lattice community tries to suppress them further by proceeding to even finer lattices, $a < 0.05$ fm.

This provides continuumlike features, which are highly welcome in general, but as a drawback it will become harder to change the topological sector. A HMC simulation may well be trapped in a single sector over a tremendously long trajectory; in particular, this is the experience in QCD simulations with dynamical overlap quarks [7]. In this case, Ref. [8] suggested a method to estimate the ratio between topologically constrained partition functions, and tested this method by determining the topological susceptibility from fixed topology overlap quark simulations.

In some circumstances it is even motivated to suppress topological transitions on purpose, in particular, when dealing with dynamical chiral fermions. In that context, configurations in a transition region cause technical problems, like a bad condition number of an overlap or domain wall Dirac operator. This can be avoided by the use of unconventional lattice gauge actions, known as "topology conserving gauge actions" [4,9] (see also Ref. [10] for a very similar formulation).

A further option is the use of a "mixed action," where one implements chiral symmetry only for the valence quarks, which requires just a moderate computational effort. In particular, overlap valence quarks have been combined with Wilson sea quarks. However, in this setup the continuum limit is not on safe ground, because (approximate) valence quark zero modes are not compensated by the sea quark spectrum [11]. This problem might be avoided by fixing the topological sector particularly to $Q = 0$.

In such settings, there are obvious questions about the (effective) ergodicity of the algorithm, since the simulation does not sample properly the entire space of all configurations. Even if we ignore this conceptual question, in practice the measurement of an observable may well be distorted. This is the issue to be addressed in this work.

Section II describes the Brower-Chandrasekharan-Negele-Wiese (BCNW) approach, and Secs. III and IV probe it in the one-dimensional O(2) and the two-dimensional O(3) nonlinear σ model. It is explored further in four-dimensional SU(2) Yang-Mills theory in Sec. V, and in the Schwinger model in Sec. VI. The field theoretic models discussed in Secs. IV–VI share fundamental features with QCD. Section VII is devoted to our conclusions.

II. THE BCNW METHOD

As a remedy against the topological freezing of Monte Carlo histories, Lüscher suggested the use of open boundary conditions, such that the topological charge can change continuously [12]. This overcomes the problem, but it breaks translational invariance[1] and one gives up integer topological charges Q. However, $Q \in \mathbb{Z}$ provides a valuable link to aspects, which are analytically known or conjectured in the continuum, for instance, regarding the ϵ regime of QCD, or properties based on an instanton picture. Therefore it is still motivated to explore alternative approaches.

In this work we maintain periodic boundary conditions (in some volume V) for the bosonic fields involved, so the topological charges Q are integers. Moreover we consider models with parity invariance. This implies $\langle Q \rangle = 0$, and the topological susceptibility is given by

$$\chi_{\rm t} = \frac{1}{V} \langle Q^2 \rangle. \tag{2.1}$$

In this framework, we are going to test the BCNW approximation [14]. It can be written in the form of an expansion in inverse powers of $V\chi_{\rm t}$,

$$\langle \mathcal{O} \rangle_Q \simeq \langle \mathcal{O} \rangle + \frac{1}{V\chi_{\rm t}} c + \frac{1}{(V\chi_{\rm t})^2} (\bar{c} - cQ^2) - \frac{2}{(V\chi_{\rm t})^3} \bar{c} Q^2. \tag{2.2}$$

The left-hand side refers to the expectation value of some observable $\mathcal{O}$ (Refs. [14] inserted specifically the pion mass) within the sectors of topological charges $\pm Q$. It is accessible even in simulations which are confined to one—or a few—topological sectors.

All the unknown terms on the right-hand side, i.e., the expectation value $\langle \mathcal{O} \rangle$, $\chi_{\rm t}$ and the coefficients c and $\bar{c}$, are quantities that asymptotically stabilize in large volume. Hence this form enables the use of results for $\langle \mathcal{O} \rangle_Q$, measured in several volumes and for distinct $|Q|$, to determine these unknown terms. In particular we are interested in $\langle \mathcal{O} \rangle$ and $\chi_{\rm t}$. The coefficients are determined as well; for instance c can be expressed by derivatives with respect to the vacuum angle θ of the extended Euclidean action $S + {\rm i}\theta Q$,

$$c = \frac{1}{2} \langle \mathcal{O} \rangle''(\theta)|_{\theta=0}, \tag{2.3}$$

but we are not going to discuss any conceivable interpretation of these coefficients.

Actually the third order in approximation (2.2) is incomplete, but the additional term in this order brings along another free parameter. These terms are identified and discussed in detail in Refs. [15–17]. Here we mostly focus on the simplest form which captures the Q dependence of $\langle \mathcal{O} \rangle_Q$, and which involves only three parameters (though an incomplete second order),

$$\langle \mathcal{O} \rangle_Q \approx \langle \mathcal{O} \rangle + \frac{c}{V\chi_{\rm t}} \left(1 - \frac{Q^2}{V\chi_{\rm t}} \right). \tag{2.4}$$

In the following, we refer to this approximation as the BCNW formula. Obviously we cannot determine the quantities $\langle \mathcal{O} \rangle, \chi_{\rm t}$ and c within a single volume; for instance

$$\langle \mathcal{O} \rangle_{Q_1} - \langle \mathcal{O} \rangle_{Q_2} \approx \frac{c}{(V\chi_{\rm t})^2} (Q_2^2 - Q_1^2) \tag{2.5}$$

only determines the ratio $c/\chi_{\rm t}^2$. If we include different volumes V_1 and V_2, however, we could use, e.g., $\langle \mathcal{O} \rangle_0(V_1) - \langle \mathcal{O} \rangle_0(V_2) \approx \frac{c}{\chi_{\rm t}} (1/V_1 - 1/V_2)$ to fix $c/\chi_{\rm t}$, and we obtain—along with relation (2.5)—all three quantities, $\langle \mathcal{O} \rangle$, $\chi_{\rm t}$ and c (we repeat that only the former two are of

[1] A recent work [13] suggests the use of P-periodic (instead of open) boundary conditions in Euclidean time, i.e., a parity flip, which also implies $Q \in \mathbb{R}$, but translation symmetry breaking effects are exponentially suppressed.

interest). In practice one would rather involve several volumes and topological sectors, and perform a three-parameter fit to the (overdetermined) system.

We distinguish three regimes for the volume V:

(i) Small volume: There are significant finite size effects of the ordinary type, not related to topology fixing, in particular, in $\langle \mathcal{O} \rangle$ and χ_t.

(ii) Moderate volume: Ordinary finite size effects are negligible (they tend to be exponentially suppressed), but $\langle \mathcal{O} \rangle_Q$ still depends significantly on $|Q|$ and V.

(iii) Large volume: There are hardly any finite size effects left; even the correction terms in approximations (2.2) and (2.4) are negligible.

In small volumes, the formulas (2.2) and (2.4) cannot be applied, because results from various volumes cannot be used for the same fit.[2] In large volumes, we obtain the correct value for $\langle \mathcal{O} \rangle$ anyhow, without worrying about frozen topology, as we see from the expansions (2.2) and (2.4). However, such large volumes may be inaccessible in realistic simulations, due to limitations of the computational resources. Hence we are interested in *moderate volumes,* where the determination of $\langle \mathcal{O} \rangle$ is difficult, but possibly feasible by means of the BCNW approximation. Moreover, that regime provides an estimate for χ_t, which is particularly hard to measure directly.

The derivation of formula (2.2) involves approximations, which assume the following:[3]

(i) $\langle Q^2 \rangle = V\chi_t$ is *large.* As we mentioned before, Eq. (2.2) takes the form of an expansion in $1/\langle Q^2 \rangle$. Once χ_t is stable, this can also be viewed as a large volume expansion.

(ii) $|Q|/\langle Q^2 \rangle$ is *small,* so we should work in the sectors with a small absolute value $|Q|$. This is less obvious from the formulas (2.2) and (2.4) (although the terms $\propto Q^2$ are related to this condition), but it is required for a step in its derivation, which relies on a stationary phase approximation.

Here we employ numerical data to explore how large $\langle Q^2 \rangle$ has to be for this approximation to be sensible, and up to which absolute value $|Q|$ the data are useful in this context. In practice it is rather easy to work at small $|Q|$, but the former condition could be a serious obstacle.

So far there have been only a few attempts to apply this approximation to simulation data. This was done for the two-flavor Schwinger model with dynamical overlap fermions [19,20] with respect to the pseudoscalar mass M_π and the chiral condensate Σ. Tests for a quantum rotor—more precisely a scalar particle on a circle with a potential—are reported in Refs. [15,16].

Another approach was derived—similarly to the BCNW approximation—in Ref. [21]. It refers to the long-distance correlation of the topological charge density $q(x)$, $Q = \int d^d x q(x)$. The applicability of that method has been tested in a set of models [22], and variants have been studied [23]. Further approaches to extract physics from topologically frozen Markov chains include Refs. [24–26]. Preliminary results of this work have been anticipated in some proceeding contributions [15,17,18,27].

[2]An extension of the BCNW approximation (2.4) *including* ordinary finite size effects has been derived in Refs. [18]. This extension can be used for fits to data obtained from small volumes. It involves, however, additional fitting parameters.

[3]For convenience, this formula has been rederived in Sec. 5.2 of Ref. [19] in a way which highlights the role of these two assumptions.

III. TESTS FOR THE QUANTUM ROTOR

As a simple but precise test, we first consider a toy model from quantum mechanics (i.e., one-dimensional quantum field theory), namely the quantum rotor, or one-dimensional XY model, or one-dimensional O(2) model. It describes a free quantum mechanical particle moving on a circle, with a periodicity condition in Euclidean time. A theoretical discussion of this system, in the continuum and for different lattice actions, is given in Ref. [28].[4] Below we write down the continuum action, and on the lattice the standard action and the Manton action [30] (in lattice units),

$$S_{\rm cont}[\varphi] = \frac{\beta_{\rm cont}}{2} \int_0^{L_{\rm cont}} dt\ \dot{\varphi}(t)^2,$$

$$S_{\rm standard}[\varphi] = \beta \sum_{t=1}^{L} (1 - \cos(\Delta\varphi_t)),$$

$$S_{\rm Manton}[\varphi] = \frac{\beta}{2} \sum_{t=1}^{L} (\Delta\varphi_t)^2. \tag{3.1}$$

$L_{\rm cont}$ and L are the extent of the periodic Euclidean time interval in the continuum and on the lattice, respectively; $\varphi(t)$ and φ_t are time dependent angles, with $\varphi(L_{\rm cont} + t) = \varphi(t)$, $\varphi_{L+t} = \varphi_t$. $\beta_{\rm cont}$ and β can be interpreted as an inverse temperature, or in this case also as the moment of inertia. In the terms for the lattice actions we define

$$\Delta\varphi_t = (\varphi_{t+1} - \varphi_t) \bmod 2\pi \in (-\pi, \pi], \tag{3.2}$$

i.e., the modulo function is implemented such that it minimizes $|\Delta\varphi_t|$. Thus $\Delta\varphi_t$ also defines the lattice topological charge density q_t (geometric definition) and the charge Q,

$$q_t = \frac{1}{2\pi} \Delta\varphi_t, \qquad Q[\varphi] = \sum_{t=1}^{L} q_t \in \mathbb{Z}. \tag{3.3}$$

[4]For the analytic treatment, Ref. [28] uses the Hamiltonian formalism. A discussion in terms of path integrals is given in Ref. [29].

In the continuum and infinite size L_{cont}, the correlation length and its product with the topological susceptibility amount to

$$\xi_{\mathrm{cont}} = 2\beta_{\mathrm{cont}}, \qquad \chi_{\mathrm{t}}\xi_{\mathrm{cont}} = \frac{1}{2\pi^2}. \tag{3.4}$$

Analytic expressions for the corresponding quantities on the lattice, with the standard action and the Manton action, are given in Ref. [28].

Our simulations were carried out with the Wolff cluster algorithm [31], which performs nonlocal update steps. This algorithm is highly efficient and provided a statistics of 5×10^9 measurements for each setting. Since it changes the topological sector frequently, in this case the observables could also be measured directly to high precision, which allows for a detailed test of the BCNW method. In most quantum field theoretic models no efficient cluster algorithm is known, in particular, in the presence of gauge fields. Then one has to resort to local update algorithms, which motivates this project, as we pointed out in Sec. I.

For our tests we set $\beta = 4$ and consider six lattice sizes in the range $L = 150\ldots400$. This is large compared to the correlation length, which was measured at $L = 400$ as

$$\xi_{\mathrm{standard}} = 6.81495(4), \qquad \xi_{\mathrm{Manton}} = 7.9989(1), \tag{3.5}$$

very close to the analytic values at $L = \infty$. This demonstrates that ordinary finite size effects are very small, but—as we are going to see—there are significant fixed topology finite size effects. Hence we are in the regime of moderate volumes, as desired. Moreover, this regime is sensible also because lattice artifacts are quite well suppressed.

The BCNW formula consists of leading terms in an expansion in $1/\langle Q^2\rangle$, cf. Sec. I. In the range $L = 150\ldots400$ we obtain

$$\langle Q^2\rangle_{\mathrm{standard}} = 1.13\ldots3.02, \qquad \langle Q^2\rangle_{\mathrm{Manton}} = 0.95\ldots2.53. \tag{3.6}$$

This suggests that we are in the transition regime to the validity of this method, which is interesting to explore.

A. Action density

We first consider the action density

$$s = \langle S\rangle/V. \tag{3.7}$$

This quantity is not directly physical, but it is suitable for testing the BCNW method, based on topologically restricted expectation values $s_{|Q|} = \langle S\rangle_{|Q|}/V$. Moreover, the corresponding fits provide a value for χ_{t}, which *is* physical.

Figure 1 shows the action density for both lattice actions under consideration, measured at fixed $|Q| = 0\ldots4$, and by including all sectors (the way the simulation samples them). The latter is constant to high accuracy for $L = 150\ldots400$, which confirms that ordinary finite size effects are negligible. On the other hand, at fixed $|Q|$ we see deviations far beyond the statistical errors, depending on L and $|Q|$, so this setting is appropriate for the application of the BCNW method.

Table I presents our results obtained by least-square fits to the BCNW approximation (2.4): we use data for $s_{|Q|}$ in all six volumes, and in the topological sectors $|Q| = 0\ldots|Q|_{\mathrm{max}}$, where $|Q|_{\mathrm{max}}$ varies from 1 to 4. Similar results are obtained when we only involve the larger volumes, such as $L = 250\ldots400$ or $300\ldots400$.

Regarding the value of s, the method works perfectly (to the given precision) for the standard action, and up to a deviation of about 0.006% for the Manton action. For the standard action the fits yield values for χ_{t}, which are again compatible with the correct value, with uncertainties around 0.05%. In the case of the Manton action a

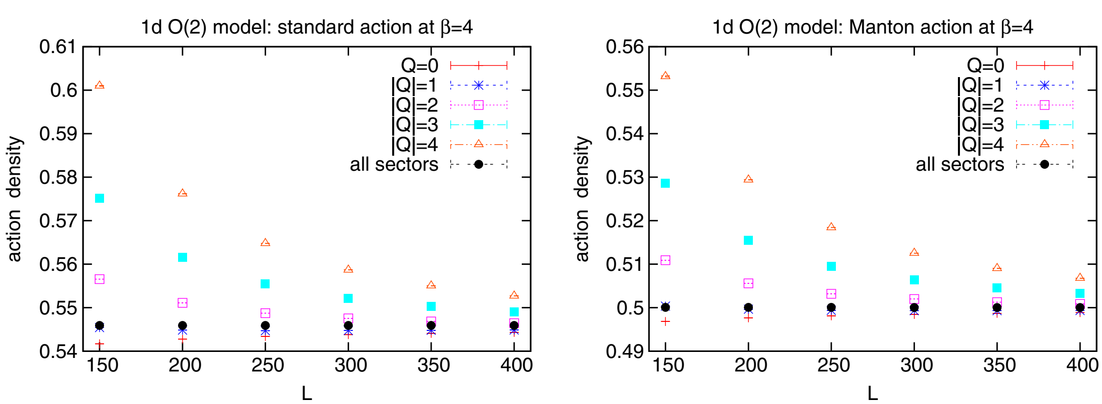

FIG. 1. The action density in the one-dimensional O(2) model at $\beta = 4$ on lattices of size $L = 150\ldots400$, with the standard action (left) and the Manton action (right). We show s measured in all sectors (which is practically constant in this range of L), as well as the values of $s_{|Q|}$ in the sectors $|Q| = 0\ldots4$, which strongly depend on $|Q|$ and V.

TABLE I. Results based on fits to the formula (2.4), with input data for the action density in the range $L = 150...400$ and $|Q| \leq |Q|_{\max}$. The last line displays s measured in all sectors at $L = 400$, and the analytic value of χ_t at $L = \infty$.

	Standard action		Manton action	
$\lvert Q\rvert_{\max}$	s	χ_t	s	χ_t
1	0.545910(1)	0.007552(4)	0.500073(3)	0.006135(9)
2	0.545910(1)	0.007555(3)	0.500072(2)	0.006132(8)
3	0.545912(2)	0.007559(5)	0.500072(2)	0.006132(8)
4	0.545912(2)	0.007559(5)	0.500072(2)	0.006131(7)
All	0.545910(1)	0.007554	0.500041(1)	0.006333

systematic discrepancy of 3% is observed, as a consequence of the approximations in formula (2.4).

In summary, this first numerical experiment can be considered a success of the BCNW method. The good results for s are highly nontrivial in view of the sizable differences in the individual sectors (shown in Fig. 1), and exactly these differences give rise to quite good estimates for χ_t. As a generic property, it is easy to measure $s_{|Q|}$ accurately (in gauge theories it is given by the mean plaquette value), so it is motivated to estimate χ_t in this way also in higher dimensional models.

B. Magnetic susceptibility

In this model, the correlation function in a fixed sector of topological charge Q has a peculiar form. For a continuous time variable t it reads [16]

$$\langle \vec{e}(0) \cdot \vec{e}(t) \rangle_Q = \frac{1}{2} \exp\left(-\frac{t(L_{\rm cont} - t)}{2\beta_{\rm cont} L_{\rm cont}} \right) \cos\left(\frac{2\pi Q t}{L_{\rm cont}} \right), \quad \text{with} \quad \vec{e}(t) = \begin{pmatrix} \cos\varphi(t) \\ \sin\varphi(t) \end{pmatrix}. \tag{3.8}$$

The unusual last factor in Eq. (3.8) obstructs the determination of a correlation length $\xi_{Q \neq 0}$, and we recall that the BCNW method does not apply to results, which are obtained in various volumes, but always at $Q = 0$.

By integrating over the time shift t, however, we obtain a quantity, which is suitable for testing this method, namely the magnetic susceptibility

$$\chi_{\rm m} = \frac{\langle \vec{M}^2 \rangle - \langle \vec{M} \rangle^2}{L_{\rm cont}} = \int_0^{L_{\rm cont}} dt\, \langle \vec{e}(0) \cdot \vec{e}(t) \rangle - \frac{1}{L_{\rm cont}} \left(\left\langle \int_0^{L_{\rm cont}} dt\, \vec{e}(t) \right\rangle \right)^2, \tag{3.9}$$

where $\vec{M} = \int_0^{L_{\rm cont}} dt\, \vec{e}(t)$ is the magnetization. The subtracted term vanishes in our case due to the global O(2) invariance, $\langle \vec{M} \rangle = \vec{0}$. The magnetic susceptibility is physical in the framework of statistical mechanics; we can interpret a configuration $[\vec{e}]$ as a spin chain. Based on Eq. (3.8) we obtain for its topologically restricted counterpart

$$\chi_{{\rm m},|Q|} = 2 \int_0^{L_{\rm cont}/2} dt \exp\left(-\frac{t}{2\beta_{\rm cont}} + \frac{t^2}{2\beta_{\rm cont} L_{\rm cont}} \right) \times \cos\left(\frac{2\pi Q t}{L_{\rm cont}} \right). \tag{3.10}$$

In each sector, the limit $L_{\rm cont} \to \infty$ leads to $\chi_{\rm m} = \chi_{{\rm m},|Q|} = 4\beta_{\rm cont}$. If we insert the large volume expansions of $\exp(t^2/(2\beta_{\rm cont} L_{\rm cont}))$ and $\cos(2\pi Q t/L_{\rm cont})$ up to $\mathcal{O}(1/L_{\rm cont}^3)$, and perform the integral, we arrive at

$$\chi_{{\rm m},Q} = \chi_{\rm m} + \frac{4\beta_{\rm cont}}{\pi^2 L_{\rm cont} \chi_t} \left(1 + \frac{3/\pi^2 - Q^2}{L_{\rm cont} \chi_t} \right) + \frac{12\beta_{\rm cont}}{\pi^4 (L_{\rm cont} \chi_t)^3} \left(\frac{5}{\pi^2} - 2Q^2 \right) + \mathcal{O}\left(\frac{1}{(L_{\rm cont} \chi_t)^4} \right), \tag{3.11}$$

where we substituted the infinite volume value $\chi_t = 1/(4\pi^2 \beta_{\rm cont})$ [28], cf. Eq. (3.4).[5] This is exactly the form of the BCNW approximation (2.2), with

$$c = \frac{4\beta_{\rm cont}}{\pi^2}, \qquad \bar{c} = \frac{12\beta_{\rm cont}}{\pi^4}, \tag{3.12}$$

and in this case the third order is complete. If we only consider the second order and neglect its $\bar{c}$ term, we are left with the BCNW approximation (2.4). A detailed derivation of the expansion (3.11) is given in the Appendix.

Therefore the magnetic susceptibility is fully appropriate for numerical tests of the validity of this approximation, where we use the corresponding lattice terms, like $\vec{M} = \sum_{t=1}^{L} \vec{e}_t$. The sources of systematic errors (errors in the BCNW approximation) are subleading finite size effects and lattice artifacts.

In analogy to Sec. III A, Fig. 2 gives an overview of the values of $\chi_{{\rm m},|Q|}$ up to $|Q| = 3$, at different L. Again we see that the value measured in all sectors is stable in L, whereas the topologically restricted results strongly depend on L and $|Q|$. Hence the setting is suitable for the BCNW method also with respect to the magnetic susceptibility.

We proceed to the fits to search the optimal values—according to formula (2.4)—for the (overdetermined) susceptibilities $\chi_{\rm m}$ and χ_t. Table II shows the results in the fitting ranges $L = L_{\min}...400$, $L_{\min} = 150, 250, 300$, and $|Q| = 0...|Q|_{\max}$, with $|Q|_{\max} = 2$ or 3.

[5] The finite size effects in χ_t, and those due to the upper bound of the integral in Eq. (3.10), are exponentially suppressed.

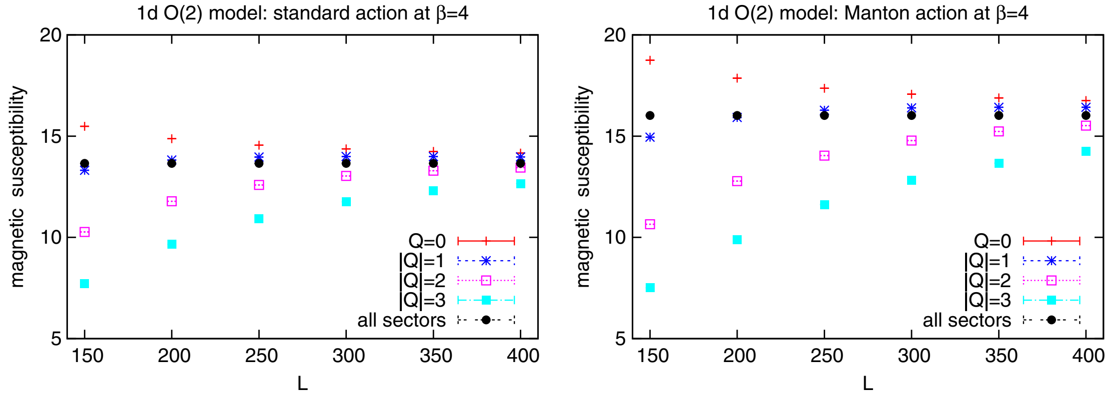

FIG. 2. The magnetic susceptibility in the one-dimensional O(2) model at $\beta = 4$ on lattices of size $L = 150\ldots400$, with the standard action (left) and the Manton action (right). We show $\chi_{\rm m}$ measured in all sectors (practically constant in this range of L), as well as $\chi_{{\rm m},|Q|}$ in the sectors $|Q| = 0\ldots3$ (well distinct).

The fitting results for both susceptibilities are compatible with the correct values, albeit the uncertainty of $\chi_{\rm t}$ is rather large. Without knowing the exact value one could combine the results of separate fits, which reduces the uncertainty, but it leads to a $\chi_{\rm t}$ value which is somewhat too small. On the other hand, for $\chi_{\rm m}$ the values are far more precise, and the relative uncertainty is on the percent level (or below) in each case. Here a combination which reduces the uncertainty is welcome, although it has to be done with care since the partial results are not independent of each other. We add that the fitting results for the coefficient c are consistent with Eq. (3.12), $c \simeq 1.6$, within (considerable) uncertainties.

The observed precisions for $\chi_{\rm m}$ and $\chi_{\rm t}$ can be understood if we consider the impact of the subleading contributions, which are missing in the BCNW formula (2.4): taking into account the additional terms up to the incomplete third order modifies the fitting results for $\chi_{\rm m}$ only on the permille level, but those for $\chi_{\rm t}$ in $\mathcal{O}(10)\%$, both with somewhat enhanced errors. Also a variety of further fitting variants, with the terms of a complete second or complete third order of approximation (3.11), with fixed or free additional terms, leads to consistent results for $\chi_{\rm m}$ and $\chi_{\rm t}$, but with enlarged errors. In summary, there seems to be no fitting strategy which improves the results compared to the simple three-parameter fit based on the BCNW approximation (2.4).

TABLE II. Results based on fits to formula (2.4), with input data for the magnetic susceptibility in the range $L = L_{\rm min}\ldots400$ and $|Q| \leq |Q|_{\rm max}$. The last line displays $\chi_{\rm m}$ measured in all sectors at $L = 400$, and $\chi_{\rm t}$ at $L = \infty$.

		Standard action		Manton action	
$L_{\rm min}$	$\lvert Q\rvert_{\rm max}$	$\chi_{\rm m}$	$\chi_{\rm t}$	$\chi_{\rm m}$	$\chi_{\rm t}$
150	2	13.64(16)	0.0072(13)	16.11(35)	0.0054(18)
150	3	13.67(22)	0.0070(22)	16.14(41)	0.0050(26)
250	2	13.64(5)	0.0071(5)	16.00(14)	0.0060(8)
250	3	13.65(13)	0.0074(15)	15.99(28)	0.0064(20)
300	2	13.64(5)	0.0071(5)	16.02(12)	0.0058(8)
300	3	13.66(13)	0.0073(17)	16.02(29)	0.0061(23)
	All	13.6545(4)	0.007554	16.0187(5)	0.006333

IV. APPLICATIONS TO THE TWO-DIMENSIONAL HEISENBERG MODEL

Our study of the two-dimensional Heisenberg model, or two-dimensional O(3) model, uses quadratic lattices of unit spacing and square-shaped volumes $V = L \times L$. On each lattice site x there is a classical spin $\vec{e}_x \in S^2$, and we implement periodic boundary conditions in both directions. We consider the standard lattice action as well as the constraint action [32],

$$S[\vec{e}]_{\rm standard} = \beta \sum_{x,\mu} (1 - \vec{e}_x \cdot \vec{e}_{x+\hat{\mu}}),$$
$$S[\vec{e}]_{\rm constraint} = \begin{cases} 0 & \vec{e}_x \cdot \vec{e}_{x+\hat{\mu}} \geq \cos\delta \quad \forall\ x, \mu = 1, 2 \\ +\infty & \text{otherwise}, \end{cases} \tag{4.1}$$

where δ is the constraint angle, and $\hat{\mu}$ is the unit vector in μ direction.

Our simulations were performed at $\beta = 1.5$ and $\delta = 0.55\pi$, respectively, with the correlation lengths

$$\text{standard action}(L = 84) \ :\ \xi = 9.42(2),$$
$$\text{constraint action}(L = 96) \ :\ \xi = 3.58(5). \tag{4.2}$$

The cluster algorithm allowed us to perform $\mathcal{O}(10^7)$ measurements at each lattice size shown in Figs. 3 and 4.

For the topological charge we use again a geometric definition [2]. To this end, each plaquette is split into two triangles, in alternating orientation. We consider the oriented solid angle of the spins at the corners of a triangle: the sum of the two angles (divided by 4π) within a plaquette

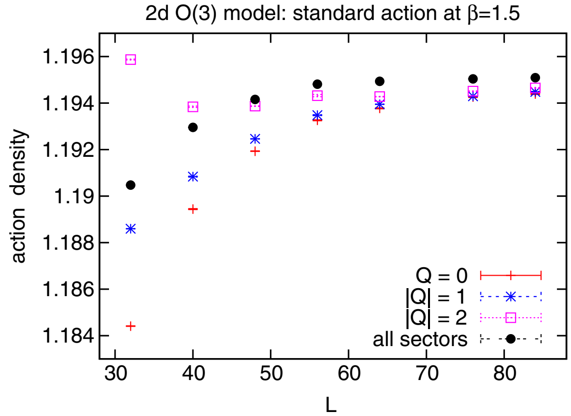

FIG. 3. The action density in the two-dimensional O(3) model, on $L \times L$ lattices with the standard lattice action, in the sectors with topological charge $|Q| = 0$, 1, 2, and summed over all sectors (i.e., all configurations used for the numerical measurements). The latter stabilizes to 0.3 permille for $L \geq 56$.

(associated with the site x) amounts to its topological charge density q_x. Due to the periodic boundary conditions, their sum must be an integer, $Q = \sum_x q_x \in \mathbb{Z}$. Details and explicit formulas are given in Refs. [22,32].

A. Action density

A study of the BCNW formula with respect to the action density (3.7) can only be performed with the standard action (in the case of the constraint action all contributing configurations have action $S_{\text{constraint}} = 0$). Figure 3 shows the values of s and $s_{|Q|}$, $|Q| \leq 2$ in the range $L = 32\ldots84$. The total expectation value s is stable within 0.0003 for $L \geq 56$, while the topologically constrained results differ by $\mathcal{O}(10^{-3})$ even at $L = 84$. Therefore $L = 56\ldots84$ is a regime of moderate volumes, which is suitable for testing the BCNW formula.

The fitting results, for $|Q| \leq 2$ and various ranges of L are listed in Table III. The fits do not match the BCNW formula perfectly, as expected, since the latter is an approximation, and the input data have very small statistical errors of $\mathcal{O}(10^{-5})$.[6] Nevertheless, the value of s is obtained correctly up to a high precision of 0.2 permille. On the other hand, the determination of the topological susceptibility is less successful; only the fit with $L = 76$ and 84 yields a result, which is correct within the errors.

B. Magnetic susceptibility and correlation length

We proceed to the constraint action (4.1) where our choice of δ yields a shorter correlation length, which favors the stabilization of observables (measured in all sectors) at

[6] Of course, the ratio χ^2/d.o.f. could be reduced by adding more terms to the $1/V$ expansion. However, in Table IV we demonstrate that this does not improve the results for the observable and for χ_t, in qualitative agreement with Sec. III.

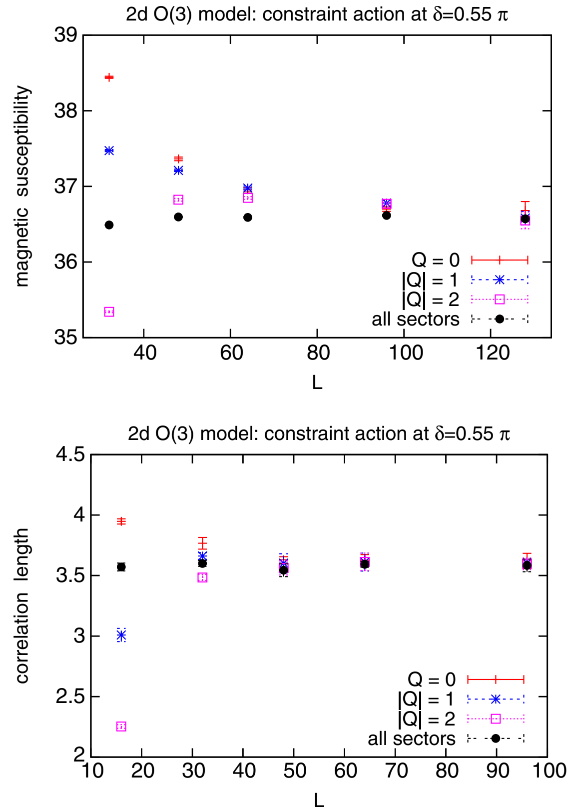

FIG. 4. Results for the magnetic susceptibility (above) and for the correlation length (below) in the two-dimensional O(3) model, with the constraint action at $\delta = 0.55\pi$. The windows, which are suitable for applications of the BCNW formula, are given by $L = 48\ldots96$ for χ_m, and by $L = 32\ldots64$ for ξ.

smaller L. This can be seen in Fig. 4, which shows the magnetic susceptibility χ_m, analogous to Eq. (3.9) (again the disconnected part vanishes due to rotational symmetry), and the correlation length ξ. Stabilization within the errors is attained for χ_m at $L \geq 48$ (with errors around 0.2 permille), and for ξ already at $L \geq 16$ [with errors of $\mathcal{O}(1)\%$]. On the other hand, for $L = 128$ the $\chi_{m,|Q|}$ values are not distinguished anymore from χ_m beyond the errors, and the same

TABLE III. Fitting results for the action density s and the topological susceptibility χ_t in the two-dimensional O(3) model. The input data in fixed topological sectors are plotted in Fig. 3.

Fitting range in L	s	χ_t	χ^2/degree of freedom
56–64	1.1955(2)	0.0035(5)	2.66
56–76	1.19538(6)	0.0031(3)	2.66
56–84	1.19536(5)	0.0030(3)	2.63
64–76	1.19532(7)	0.0031(3)	2.65
64–84	1.19531(5)	0.0031(3)	2.58
76–84	1.1953(1)	0.0026(3)	2.60
$L = 84$, all sectors	1.195089(5)	0.002323(3)	

TABLE IV. Fitting results based on data for χ_m and for ξ in the two-dimensional O(3) model, in fitting ranges $L_{\min}$–$L_{\max}$, and sectors with $|Q| \leq 2$. In the case of χ_m, with the optimal range, we show results for the BCNW approximation (2.4), as well as its extension to the complete second order plus one term of $\mathcal{O}(1/V^3)$, according to formula (2.2).

	Fitting range	BCNW formula	Incomplete third order	All sectors at $L_{\max}$
χ_m	48–64	36.56(4)	36.64(11)	36.590(9)
χ_t		0.0026(2)	0.0031(6)	0.0027935(14)
χ_m	48–96	36.58(3)	36.64(7)	36.616(9)
χ_t		0.0026(2)	0.0032(6)	0.0027942(11)
ξ	32–64	3.56(2)	3.58(4)	3.59(2)
χ_t		0.0027(3)	0.0034(14)	0.0027935(14)

happens for $\xi_{|Q|}$ already at $L = 96$. Finally, we have to exclude $L = 16$, because here we only obtain $\langle Q^2 \rangle \simeq 0.63$; hence its inverse is not suitable as an expansion parameter. This singles out the regime of moderate volumes, where the BCNW formula is appropriate, to the range $L = 48 \ldots 96$ for χ_m, and $L = 32 \ldots 64$ for ξ.

Our fitting results are given in Table IV. In the case of χ_m we probe the BCNW formula (2.4) [with its incomplete second order, $\mathcal{O}(1/V^2)$], as well as its extensions to the second order plus an incomplete third order as given in formula (2.2). For the latter option, the approximation is more precise, but an additional free parameter $\bar{c}$ hampers the fits.

For both fitting versions, the results for χ_m and χ_t are compatible with the directly measured values. We observe, however, that the inclusion of terms beyond the BCNW formula enhances the uncertainty (due to the additional fitting parameter). The uncertainty is on the permille level for χ_m, but large for χ_t, in particular, with extra terms. (Without these terms it is around 8%.) It turns out to be nonprofitable to extend the approximation beyond the BCNW formula.

The simple BCNW approximation is also superior for the fits with respect to ξ, where the additional terms drastically increase the uncertainty. The results in Table IV are correct, within percent level for ξ, but again with a large uncertainty of the χ_t value.

We add that we also tried fits to the complete second order approximation, without the third order term that appears in formula (2.2). However, this scenario (which also involves the fitting parameter $\bar{c}$) is clearly unfavorable: in this case, it often happens that the least-square fit even fails to converge to values in the correct magnitude.

To conclude, this study suggests that the simple BCNW formula, with only three free parameters, is in fact optimal for extracting values for the considered observable, and for χ_t. Moreover, we confirm that the method works best for the determination of the observable; it is less successful with respect to the determination of χ_t.

V. RESULTS IN FOUR-DIMENSIONAL SU(2) YANG-MILLS THEORY

The topological tunneling rate has been investigated in four-dimensional Yang-Mills theories with the heat bath [33] and the HMC algorithm [34]. In both cases the autocorrelation time with respect to Q was found to increase drastically for decreasing lattice spacing, which further substantiates the motivation of our study.

A. Simulation setup

We consider four-dimensional SU(2) Yang-Mills theory, which has the continuum action

$$S_{\text{cont}}[A] = \beta_{\text{cont}} \int d^4x \; F^a_{\mu\nu}(x) F^a_{\mu\nu}(x), \tag{5.1}$$

and the topological charge

$$Q[A] = \frac{1}{16\pi^2} \int d^4x \; \epsilon_{\mu\nu\rho\sigma} F^a_{\mu\nu}(x) F^a_{\rho\sigma}(x). \tag{5.2}$$

On the lattice we simulate Wilson's standard plaquette action. For the topological charge of a lattice gauge configuration $[U]$, we use an improved field theoretic definition [3],

$$Q[U] = \frac{1}{16\pi^2} \sum_x \epsilon_{\mu\nu\rho\sigma} \sum_{\Box=1,2,3} \frac{c_\Box}{\Box^4} F^{(\Box\times\Box)}_{x,\mu\nu}[U] F^{(\Box\times\Box)}_{x,\rho\sigma}[U], \tag{5.3}$$

where $F^{(\Box\times\Box)}_{x,\mu\nu}[U]$ denotes the lattice field strength tensor, clover averaged over square-shaped loops of size $\Box \times \Box$, and $(c_1, c_2, c_3) = (1.5, -0.6, 0.1)$. Before applying Eq. (5.3), we perform a number of cooling sweeps with the intention of removing local fluctuations in the gauge configurations, while preserving the topological structure.

A cooling sweep amounts to a local minimization of the action, i.e., a minimization with respect to each gauge link within a short range. For this minimization we use again an improved lattice Yang-Mills action,

$$S[U] = \frac{\beta}{16} \sum_x \sum_{\mu\nu} \sum_{\Box=1,2,3} \frac{c_\Box}{\Box^4} \text{Tr}(\mathbb{1} - W^{(\Box\times\Box)}_{x,\mu\nu}[U]), \tag{5.4}$$

where $W^{(\Box\times\Box)}_{x,\mu\nu}[U]$ is a clover averaged loop of size $\Box \times \Box$ with the coefficients $c_\Box$ given above [for comparison, the standard plaquette action corresponds to $(c_1, c_2, c_3) = (1, 0, 0)$]. Choosing an appropriate number of cooling sweeps is a subtle and somewhat ambiguous task, which is carried out for each gauge configuration one by one. After every cooling sweep we compute $Q[U]$ according to Eq. (5.3). As soon as $Q[U]$ is stable (it varies by less than 10% and is close to an integer for at least 50 cooling

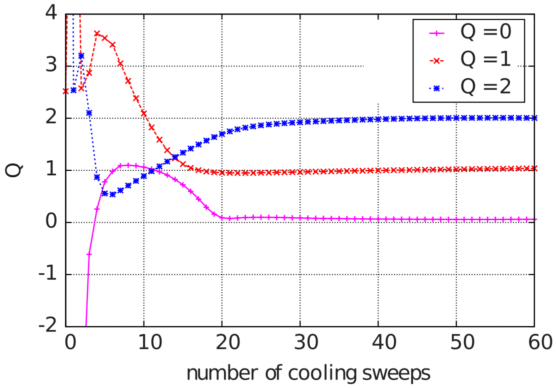

FIG. 5. Cooling and assignment of the topological charge for three typical gauge configurations, at $\beta = 2.5$, in a lattice volume $V = 18^4$.

sweeps), the corresponding close integer is the topological charge that we assign to the gauge configuration $[U]$. Figure 5 shows examples for typical cooling histories of gauge configurations with $Q = 0$, 1 and 2. (Details of this procedure, and a comparison to other definitions of the topological charge, are discussed in Ref. [6].)

Our simulations were performed with a heat bath algorithm; see, e.g., Ref. [35]. We set $\beta = 2.5$, which corresponds to a lattice spacing $a \approx 0.073$ fm, if the scale is set with the QCD Sommer parameter $r_0 = 0.46$ fm [36]. This value is in the range of lattice spacings 0.05 fm $\lesssim a \lesssim 0.15$ fm typically used in contemporary QCD simulations. We generated gauge configurations in lattice volumes $V = L^4$, with $L = 12, 14, 15, 16, 18$.[7] In each volume, observables were measured on 4000 configurations, separated by 100 heat bath sweeps. This guarantees their statistical independence; in particular, even the autocorrelation time with respect to the topological charge Q is below 20 heat bath sweeps.

B. Computation of observables

The observable we focus on is the static quark-antiquark potential $\mathcal{V}_{q\bar{q}}(r)$ for separations $r = 1, 2 \ldots 6$. This quantity can be interpreted as the mass of a static-static meson. To determine $\mathcal{V}_{q\bar{q}}(r)$, we consider temporal correlation functions of operators

$$O_{q\bar{q}}(r) = \bar{q}(\vec{r}_1) U^{\mathrm{APE}}(\vec{r}_1, \vec{r}_2) q(\vec{r}_2), \quad r = |\vec{r}_1 - \vec{r}_2|, \quad (5.5)$$

where $\bar{q}$, q represent spinless static quarks, while $U^{\mathrm{APE}}(\vec{r}_1, \vec{r}_2)$ denotes a product of APE smeared spatial links [37] along a straight line connecting the lattice sites $\vec{r}_1$ and $\vec{r}_2$ on a given time slice. For the quarks we use the HYP2 static action [38], which is designed to reduce UV fluctuations and, therefore, to improve the signal-to-noise ratio. These temporal correlation functions can be simplified analytically resulting in Wilson loop averages $\langle W(r,t) \rangle$ with APE smeared spatial and HYP2 smeared temporal lines of length r and t, respectively. Thus we arrive at the vacuum expectation value,

$$\langle \Omega | O^{\dagger}_{\bar{q}q}(t) O_{\bar{q}q}(0) | \Omega \rangle \propto \langle W(r,t) \rangle. \quad (5.6)$$

We chose the APE smearing parameters as $N_{\mathrm{APE}} = 15$ and $\alpha_{\mathrm{APE}} = 0.5$, which (roughly) optimizes the overlap of $O_{\bar{q}q}|\Omega\rangle$ with the ground state of the static potential (for details of the smearing procedure we refer to Ref. [39], where a similar setup had been used).

C. Numerical results

1. The static potential

Figure 6 shows results for the static potential measured in all topological sectors, i.e., for each r and t the Wilson loop average is computed on all configurations, which are available in some volume.[8] The volumes 14^4, 15^4, 16^4 and 18^4 yield identical results within statistical errors, but the static potential in the 12^4 volume differs by several σ for quark-antiquark separations $r \geq 3$. We conclude that $V = 12^4$ entails sizable ordinary finite volume effects (not associated with topology fixing), whereas for volumes $V \geq 14^4$ such ordinary finite volume effects are negligible. Consequently, we do not use the 12^4 lattice in the following fixed topology studies.[9]

For $V = 15^4$, Fig. 7 demonstrates that static potentials obtained at fixed topology from different sectors $|Q| = 0 \ldots 5$ (by averaging only over configurations of a fixed charge $|Q|$), $\mathcal{V}_{q\bar{q},|Q|}$, differ significantly.[10] For example, $\mathcal{V}_{q\bar{q},0}(r = 6)$ and $\mathcal{V}_{q\bar{q},4}(r = 6)$ differ by more than 6σ. They are also well distinct from the corresponding result in all sectors, $\mathcal{V}_{q\bar{q},|Q|\leq 1}(6) < \mathcal{V}_{q\bar{q}}(6) < \mathcal{V}_{q\bar{q},|Q|\geq 2}(6)$. These observations show that $V = 14^4 \ldots 18^4$ is in the regime that we denoted as *moderate volumes* (cf. Sec. II), where the BCNW method is appropriate to extract observables from fixed topology measurements. Similar results for the static potential in SU(3) Yang-Mills theory have been reported in Ref. [4].

To extract the physical static potential from Wilson loop averages, separately computed in distinct topological sectors $|Q| \leq 7$ and some volume V, $\langle W_V(r,t) \rangle_{|Q|}$, we follow the procedure discussed in Ref. [15].

[7] Unless stated otherwise, we continue using lattice units.

[8] As usual, we determined $\mathcal{V}_{q\bar{q}}(r)$ by searching for a plateau value of the effective mass $m_{\mathrm{eff}}(r,t) = \log(\langle W(r,t+1) \rangle / \langle W(r,t) \rangle)$.

[9] We repeat that the BCNW formula can be extended by incorporating ordinary finite volume effects [18].

[10] Again we determined $\mathcal{V}_{q\bar{q}}(r)$ by fitting constants to effective mass plateaus. Even though topology has been fixed, the effective masses exhibit a constant behavior (within statistical errors) at large t.

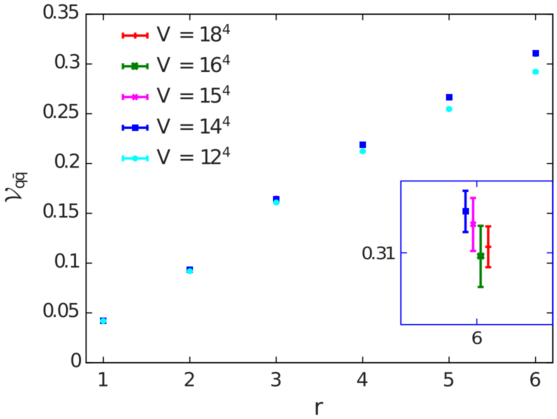

FIG. 6. The static potential $\mathcal{V}_{q\bar{q}}(r)$ in a variety of lattice volumes $V = 12^4 \ldots 18^4$.

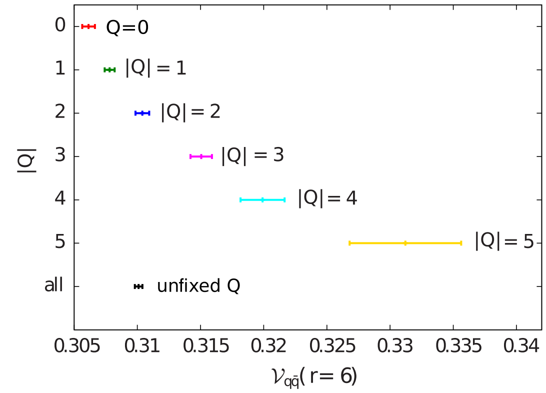

FIG. 7. The static potential at separation $r = 6$, $\mathcal{V}_{q\bar{q}}(6)$, for fixed topological sectors $|Q| \leq 5$, and without topology fixing, in the volume $V = 15^4$.

(i) We perform χ^2 minimizing fits of either the $1/V$ expansion of the correlation function [14],

$$C_{Q,V}(t) = \langle W_V(r,t)\rangle_{|Q|} \approx \alpha(r)\exp\left\{-\left[\mathcal{V}_{q\bar{q}}(r) + \frac{1}{2}\mathcal{V}''_{q\bar{q}}(r)\frac{1}{V\chi_t}\left(1 - \frac{Q^2}{V\chi_t}\right)\right]t\right\} \quad (5.7)$$

[cf. formula (2.4)], or of the improved approximation [16],

$$C_{Q,V}(t) \simeq \frac{\alpha(r)}{\sqrt{1 + \mathcal{V}''_{q\bar{q}}(r)t/(\chi_t V)}} \times \exp\left(-\mathcal{V}_{q\bar{q}}(r)t - \frac{1}{\chi_t V}\left(\frac{1}{1 + \mathcal{V}''_{q\bar{q}}(r)t/(\chi_t V)} - 1\right)\frac{1}{2}Q^2\right) \quad (5.8)$$

with respect to the parameters $\mathcal{V}_{q\bar{q}}(r)$, $\mathcal{V}''_{q\bar{q}}(r) = \partial^2_\theta \mathcal{V}_{q\bar{q}}(r,\theta)|_{\theta=0}$, $\alpha(r)$ $(r = 1 \ldots 6)$ and χ_t to the numerical results for $\langle W_V(r,t)\rangle_{|Q|}$ in the range $t_{\min} \leq t \leq t_{\max}$, where $t_{\min}$ and $t_{\max}$ are displayed in Table V.[11] When fitting formula (5.8), we also study the scenario where χ_t is fixed to $\chi_t = 7 \times 10^{-5}$, which was obtained in Ref. [3] by means of a direct measurement, in agreement with the fixed topology study in Ref. [22]. Moreover, we checked that the resulting fit parameters are stable within errors when we vary $t_{\min}$ and $t_{\max}$ by ± 1.

(ii) The results for $\langle W_V(r,t)\rangle_{|Q|}$ entering the fit are restricted to those $|Q|$ and V values for which $1/(\chi_t V), |Q|/(\chi_t V) < 1$ or < 0.5; we recall that the approximations (5.7) and (5.8) are only valid for sufficiently large $\chi_t V = \langle Q^2\rangle$, and small $|Q|$. To implement this selection we insert $\chi_t = 7 \times 10^{-5}$ [3]; Table V gives an overview.

(iii) We either perform a single combined fit to all considered separations $r = 1 \ldots 6$, or six separate fits, one for each r. In the latter case we obtain six results for χ_t, which agree within the errors in most cases, cf. Sec. V C 2.

Table VI collects the results for $\mathcal{V}_{q\bar{q}}(r)$ from fixed topology computations (using four volumes, $V = 14^4$, 15^4, 16^4, 18^4), and computed in all sectors at $V = 18^4$. There is agreement between most of these results within about 2σ. Only for $r = 1$, and the relaxed constraint $1/(\chi_t V), |Q|/(\chi_t V) < 1$, there are a few cases with discrepancies beyond 3σ, in particular, for the expansion (5.7) (the corresponding data in Table VI are displayed in italics).

The extent of the errors of the fitting results is fairly independent of the choice of the expansion [(5.7), (5.8), or (5.8) with $\chi_t = 7 \times 10^{-5}$ fixed]. The errors increase,

TABLE V. Temporal fitting ranges $t_{\min} \ldots t_{\max}$, and maximum topological charges $|Q|$, for the lattice volumes V under consideration.

V	$t_{\min}$	$t_{\max}$	Maximum $\lvert Q\rvert$ fulfilling $1/(\chi_t V)$, $\lvert Q\rvert/(\chi_t V) < 1$	Maximum $\lvert Q\rvert$ fulfilling $1/(\chi_t V)$, $\lvert Q\rvert/(\chi_t V) < 0.5$
14^4	5	7	2	1
15^4	5	7	3	1
16^4	5	8	4	2
18^4	5	8	7	3

[11] Again, θ is the vacuum angle that we referred to before in Eq. (2.3).

TABLE VI. Results for the static potential $\mathcal{V}_{q\bar{q}}(r)$ for separations $r = 1\ldots6$ measured with and without topology fixing. In the column Method the equation number of the expansion is listed, c denotes a single *combined* fit for all separations $r = 1\ldots6$, s denotes a *separate* fit for each separation, and χ_t indicates that the topological susceptibility is not a fit parameter, but fixed to $\chi_t = 7\times10^{-5}$. Fixed topology results, which differ by more than 3σ from the directly computed value, are written in italics.

Method	$\mathcal{V}_{q\bar{q}}(1)$	$\mathcal{V}_{q\bar{q}}(2)$	$\mathcal{V}_{q\bar{q}}(3)$	$\mathcal{V}_{q\bar{q}}(4)$	$\mathcal{V}_{q\bar{q}}(5)$	$\mathcal{V}_{q\bar{q}}(6)$
			All sectors, $V = 18^4$			
	0.04229(1)	0.09329(2)	0.1646(1)	0.2190(1)	0.2664(2)	0.3101(3)
			Fixed topology, $V \in \{14^4, 15^4, 16^4, 18^4\}$, $1/(\chi_t V), \lvert Q\rvert/(\chi_t V) < 1$			
(5.7)c	*0.04240(3)*	0.09343(8)	0.1646(2)	0.2189(3)	0.2662(4)	0.3097(5)
(5.7)s	*0.04241(3)*	0.09342(9)	0.1646(2)	0.2189(3)	0.2662(4)	0.3097(6)
(5.8)c	0.04230(3)	0.09324(8)	0.1644(2)	0.2187(3)	0.2661(4)	0.3098(6)
(5.8)s	*0.04240(3)*	0.09338(9)	0.1645(2)	0.2188(3)	0.2661(4)	0.3098(6)
(5.8)cχ_t	0.04225(3)	0.09326(8)	0.1643(2)	0.2186(3)	0.2660(4)	0.3097(6)
(5.8)sχ_t	0.04225(3)	0.09326(8)	0.1643(2)	0.2186(3)	0.2660(4)	0.3097(6)
			Fixed topology, $V \in \{14^4, 15^4, 16^4, 18^4\}$, $1/(\chi_t V), \lvert Q\rvert/(\chi_t V) < 0.5$			
(5.7)c	0.04227(4)	0.09326(14)	0.1645(3)	0.2190(5)	0.2665(7)	0.3103(10)
(5.7)s	0.04226(4)	0.09322(13)	0.1644(3)	0.2189(5)	0.2666(8)	0.3105(11)
(5.8)c	0.04227(4)	0.09326(14)	0.1645(4)	0.2190(5)	0.2665(7)	0.3104(10)
(5.8)s	0.04226(4)	0.09323(13)	0.1645(3)	0.2189(5)	0.2665(8)	0.3104(10)
(5.8)cχ_t	0.04225(4)	0.09317(12)	0.1643(3)	0.2186(4)	0.2660(6)	0.3096(8)
(5.8)sχ_t	0.04225(3)	0.09317(12)	0.1643(3)	0.2186(4)	0.2660(6)	0.3096(8)

however, by factors up to ≈2, when we implement the stringent constraint $1/(\chi_t V), |Q|/(\chi_t V) < 0.5$, which is expected, since less input data are involved; see Table V. All fits of the expansions (5.7) and (5.8) capture well the fixed topology results.

For the extraction of the potential it seems essentially irrelevant whether a single combined fit or six separate fits are performed. Both the mean values and the statistical errors of $\mathcal{V}_{q\bar{q}}(r)$ are in most cases very similar. A single combined fit, however, seems somewhat advantageous regarding the determination of χ_t; see Sec. V C 2.

Figure 8 compares the static potential obtained from fixed topology Wilson loops, and computed without topology fixing at $V = 18^4$. As reflected by Table VI there is excellent agreement within the errors.

The expansion (5.7) of fixed topology Wilson loop averages $\langle W_V(r,t)\rangle_{|Q|}$ is a decaying exponential in t. This suggests defining a static potential at fixed topological charge $|Q|$ and volume V,

$$\mathcal{V}_{q\bar{q},|Q|,V}(r) = -\frac{d}{dt}\ln\left(\left\langle W_V(r,t)\right\rangle_{|Q|}\right), \qquad (5.9)$$

for some value of t, where formula (5.7) is a rather precise approximation. Within statistical errors $\mathcal{V}_{q\bar{q},|Q|,V}(r)$ is independent of t for $t_{\min} \le t \le t_{\max}$. Therefore, we determine $\mathcal{V}_{q\bar{q},|Q|,V}(r)$ by a χ^2 minimizing fit of a constant to the right-hand side of Eq. (5.9), with the derivative replaced by a finite difference (this is the common definition of an effective mass) in the interval $t_{\min} \le t \le t_{\max}$. For $|Q| = 0\ldots4$ and $V = 14^4$, 15^4, 16^4, 18^4, the values for $\mathcal{V}_{q\bar{q},|Q|,V}(r=6)$ are plotted in Fig. 9.

As already shown in Fig. 7, there is a strong dependence on the topological sector, which becomes increasingly prominent for smaller volumes. From expansion (5.7) the fixed topology static potential is expected to behave as

$$\mathcal{V}_{q\bar{q},|Q|,V}(r) \approx \mathcal{V}_{q\bar{q}}(r) + \frac{1}{2}\mathcal{V}''_{q\bar{q}}(r)\frac{1}{V\chi_t}\left(1 - \frac{Q^2}{V\chi_t}\right). \qquad (5.10)$$

The corresponding curves for $|Q| = 0\ldots4$, with parameters $\mathcal{V}_{q\bar{q}}(r=6)$, $\mathcal{V}''_{q\bar{q}}(r=6)$ and χ_t determined by the

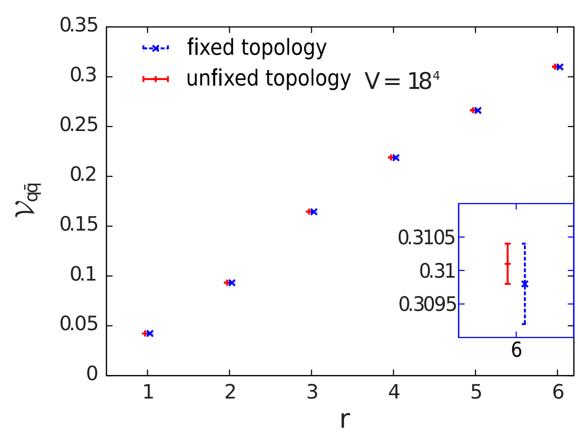

FIG. 8. Comparison of static potential obtained from fixed topology Wilson loops, in the volumes $V = 14^4$, 15^4, 16^4, 18^4, with $1/(\chi_t V), |Q|/(\chi_t V) < 1$, using expansion (5.8) with one combined fit, and directly measured at $V = 18^4$. (Since unfixed and fixed topology results coincide within the errors, they are shifted horizontally for better visibility.)

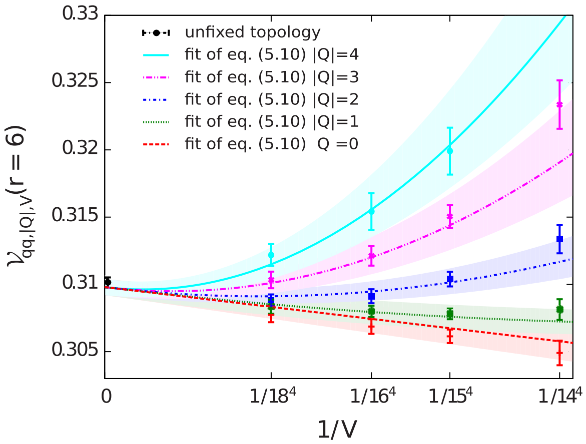

FIG. 9. The fixed topology static potential $\mathcal{V}_{q\bar{q},Q,V}(r=6)$ for $|Q| = 0\ldots4$, as a function of $1/V$, and the curves corresponding to approximation (5.10).

previously discussed fits [$V = 14^4\ldots18^4$, $1/(\chi_t V), |Q|/(\chi_t V) < 1$, expansion (5.7) and a single combined fit], are also shown in Fig. 9. One clearly sees that approximation (5.10) nicely describes the numerical results for $\mathcal{V}_{q\bar{q},|Q|,V}(r=6)$.

We conclude that one can obtain a correct and accurate physical static potential from Wilson loops separately computed in different topological sectors. The errors are larger by factors $\approx 2\ldots5$ (cf. Table VI) for a fixed topology computation using four ensembles, compared to a corresponding direct computation using a single ensemble ($V = 18^4$).

2. *The topological susceptibility*

In Table VII we present results for the topological susceptibility extracted from fixed topology Wilson loops $\langle W_V(r,t)\rangle_{|Q|}$. Again we use the $1/V$ expansion (5.7) or (5.8), the constraints $1/(\chi_t V), |Q|/(\chi_t V) < 1$ or < 0.5, and either a single combined fit to all considered separations $r = 1\ldots6$ or six separate fits, one for each r. The latter yields six different results for χ_t.

Not all of the extracted χ_t values perfectly agree with each other or with the result $\chi_t = (7.0 \pm 0.9) \times 10^{-5}$ from Ref. [3], which we take as a reference. Using the weak constraint $1/(\chi_t V), |Q|/(\chi_t V) < 1$ there seems to be a slight tension in the form of $\approx 2\sigma$ discrepancies, when performing fits with formula (5.7). The extended expansion (5.8) gives somewhat better results: no tension shows up, and most results agree with the reference value within σ.

One might hope for further improvement by using the stronger constraint $1/(\chi_t V), |Q|/(\chi_t V) < 0.5$, since then formulas (5.7) and (5.8) are more accurate. Indeed this leads to consistency with the reference value, but in most cases the errors are very large, of the order of 100% or even more. For this strong constraint the available $\mathcal{V}_{q\bar{q},|Q|}$ data are not sufficient to extract a useful result for χ_t. Note that here the error for one combined fit is significantly smaller than those for the separate fits.

We conclude that—in principle—one can extract the topological susceptibility in Yang-Mills theory from the static potential at fixed topology using formulas like (5.7) or (5.8). In practice, however, one needs precise data in several large volumes. Only when a variation of the input data [e.g., by using different bounds with respect to $1/(\chi_t V), |Q|/(\chi_t V)$] leads to precise and stable χ_t values should one consider the result trustworthy. The data used in this work are not sufficient to achieve this standard. As we mentioned before, more promising methods to determine χ_t from simulations at fixed topology using the same lattice setup have recently been explored [22–24,26].

VI. RESULTS IN THE SCHWINGER MODEL

A. Simulation setup

We proceed to the Schwinger model—or two-dimensional quantum electrodynamics—as a test model with dynamical fermions. This model has the continuum Lagrangian

TABLE VII. Results for the topological susceptibility $\chi_t \times 10^5$ from fixed topology computations of the static potential $\mathcal{V}_{q\bar{q}}(r)$ for various separations $r = 1\ldots6$. In the column Method the equation number of the expansion is listed, c denotes a single combined fit for all separations $r = 1\ldots6$, and s denotes a separate fit for each separation. The reference value from a direct computation is $\chi_t \times 10^5 = (7.0 \pm 0.9)$ [3].

Method	$\mathcal{V}_{q\bar{q}}(1)$	$\mathcal{V}_{q\bar{q}}(2)$	$\mathcal{V}_{q\bar{q}}(3)$	$\mathcal{V}_{q\bar{q}}(4)$	$\mathcal{V}_{q\bar{q}}(5)$	$\mathcal{V}_{q\bar{q}}(6)$
Fixed topology, $V \in \{14^4, 15^4, 16^4, 18^4\}$, $1/(\chi_t V), \lvert Q\rvert/(\chi_t V) < 1$						
(5.7)c	8.8(0.5)					
(5.7)s	8.8(0.5)	8.7(0.6)	8.6(0.7)	8.6(0.9)	8.8(1.0)	8.9(1.2)
(5.8)c	7.1(0.6)					
(5.8)s	8.6(0.5)	8.2(0.7)	7.7(0.8)	7.3(0.9)	7.0(1.0)	6.7(1.1)
Fixed topology, $V \in \{14^4, 15^4, 16^4, 18^4\}$, $1/(\chi_t V), \lvert Q\rvert/(\chi_t V) < 0.5$						
(5.7)c	11.8(5.9)					
(5.7)s	10.0(14.0)	20.7(44.3)	11.1(8.2)	11.8(16.0)	12.8(8.7)	15.4(52.1)
(5.8)c	11.9(5.4)					
(5.8)s	10.2(21.8)	10.7(12.5)	11.3(8.7)	11.8(5.8)	13.0(9.7)	14.6(12.2)

$$\mathcal{L}_{\mathrm{cont}}(\psi,\bar{\psi},A) = \sum_{\mathrm{f}=1}^{N_\mathrm{f}} \bar{\psi}^{(\mathrm{f})}\left(\gamma_\mu(\partial_\mu + \mathrm{i}g_{\mathrm{cont}}A_\mu) + m^{(\mathrm{f})}\right)\psi^{(\mathrm{f})} + \frac{1}{4}F_{\mu\nu}F_{\mu\nu}, \tag{6.1}$$

where N_f is the number of fermion flavors. It is a widely used toy model, which shares important features with QCD. In particular, the U(1) gauge theory in two (spacetime) dimensions allows for topologically nontrivial gauge configurations, similar to instantons in four-dimensional Yang-Mills theories and in QCD. The topological charge is given by

$$Q[A] = \frac{1}{\pi}\int d^2x\ \epsilon_{\mu\nu}F_{\mu\nu}. \tag{6.2}$$

Moreover, for $N_\mathrm{f} = 2$ the low lying energy eigenstates contain a light iso-triplet composed of quasi-Nambu-Goldstone bosons, which we denote as pions. This model also exhibits fermion confinement.

We simulated the Schwinger model on periodic lattices of volume $V = L \times L$ (as before we use lattice units), with $N_\mathrm{f} = 2$ mass degenerate flavors. They are represented by Wilson fermions, and we use the standard plaquette gauge action (see, e.g., Ref. [40]).

One can approach the continuum limit by increasing L, while keeping the terms gL and $M_\pi L$ fixed, where M_π denotes the pion mass.[12] This requires decreasing both g and M_π proportional to $1/L$ (for the latter the fermion mass has to be adjusted). It is also common to refer to $\beta = 1/g^2$, in analogy to the previous sections.

As in Secs. III and IV, we employ a geometric definition of the topological charge on the lattice [41],

$$Q[U] = \frac{1}{2\pi}\sum_P \phi(P), \tag{6.3}$$

where $\sum_P$ denotes the sum over all plaquettes $P = e^{\mathrm{i}\phi(P)}$, $-\pi < \phi(P) \leq \pi$. With this definition, $Q \in \mathbb{Z}$ holds for any stochastic gauge configuration.

We performed simulations at various values of β, m and L using the HMC algorithm of Ref. [42], with multiple time scale integration and mass preconditioning [43]. We started with rather short simulations (≈50000…100000 HMC trajectories) on small lattices ($L = 8…28$), to investigate the transition probability between topological sectors per HMC trajectory. This probability is plotted in Fig. 10, as a function of $g = 1/\sqrt{\beta}$ and m/g, while $gL = 24/\sqrt{5}$ is kept constant. (The ratio m/g is proportional to the bare fermion mass in physical units.) As expected, topological transitions are frequent at large couplings g (coarse lattices), whereas at weak coupling (fine lattices) topology freezing is observed. Such a freezing is also observed in QCD, which is the main motivation of this work. We see that the dependence of the transition probability on the ratio m/g, and therefore on the dimensional bare fermion mass, is rather weak.

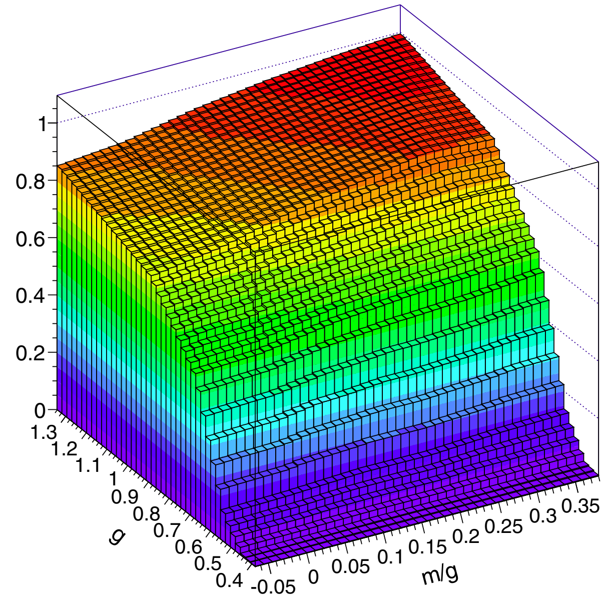

FIG. 10. The transition probability to a different topological sector per HMC trajectory as a function of $g = 1/\sqrt{\beta}$ (varying the lattice spacing in physical units, $a \propto g$) and m/g (varying the bare fermion mass in physical units) at $gL = 24/\sqrt{5}$ (fixed dimensional volume and coupling constant).

Similarly to the previous two sections we now explore the possibility of extracting physical energy levels (the "hadron" masses in the Schwinger model) from simulations at fixed topology. To obtain such results with small statistical errors, we focus on a single coupling and a single quark mass,

$$\beta = 4, \qquad m = 0.1, \tag{6.4}$$

and we perform long simulations (≈500000 HMC trajectories) for volumes $V = L \times L$, with $L = 40$, 44, 48, 52, 56, 60.

B. Computation of observables

We determine the topological charge $Q[U]$ for each gauge configuration U according to definition (6.3). (To measure observables at fixed topological charge ν, we only use the configurations with $Q[U] = \nu$.)

The hadron masses that we investigate are the static potential $\mathcal{V}_{\bar{q}q}(r)$, which has been discussed before in Yang-Mills theory (Sec. V B), and the pion mass M_π. A suitable pion creation operator reads

[12] In physical units, g has the dimension of a mass, so these products are both dimensionless. This also introduces a dimensional lattice spacing $a \propto g$.

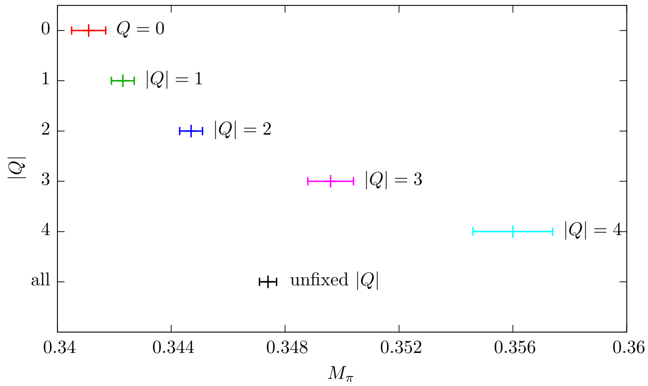

FIG. 11. The pion masses $M_{\pi,|Q|}$ in distinct topological sectors $|Q| = 0 \ldots 4$, and M_π obtained in all sectors, in the volume $V = 40^2$.

$$O_\pi = \sum_x \bar{\psi}_x^{(u)} \gamma_3 \psi_x^{(d)}, \tag{6.5}$$

where u and d label the two (degenerate) fermion flavors.[13] For the static potential we use again

$$O_{q\bar{q}} = \bar{q}(r_1)U(r_1; r_2)q(r_2), \qquad r = |r_1 - r_2|. \tag{6.6}$$

Also here $\bar{q}$ and q represent spinless static fermions and $U(r_1; r_2)$ denotes the product of spatial links connecting the lattice sites r_1 and r_2 on a given time slice. Since there is only one spatial dimension, we do not apply any gauge link smearing.

C. Numerical results

1. The pion mass and the static potential

Similar to Eq. (5.9) one can define a pion mass at fixed topological charge $|Q|$ and volume V by

$$M_{\pi,|Q|,V} = -\frac{d}{dt} \ln\left(\left\langle O_\pi^\dagger(t) O_\pi(0) \right\rangle\right) \tag{6.7}$$

for some value of t, where approximation (5.7) is quite precise. Within statistical errors, $M_{\pi,|Q|,V}$ is independent of t for large t. Therefore, we determine $M_{\pi,|Q|,V}$ by a χ^2 minimizing fit of a constant to the right-hand side of Eq. (6.7) (with the derivative replaced by a finite difference).

Figure 11 shows that pion masses obtained at fixed topology in different topological sectors, $M_{\pi,|Q|}$, differ significantly at $V = 40^2$. For example, $M_{\pi,0}$ and $M_{\pi,3}$ differ by more than 6σ. The physically meaningful value measured in all sectors, M_π, also deviates, e.g., from $M_{\pi,0}$ by more than 7σ. Figure 11 demonstrates also here the necessity to analytically assemble fixed topology results, when the Monte Carlo algorithm is unable to generate frequent changes in Q.

[13] For an introduction about the construction of hadron creation operators, see, e.g., Ref. [44].

TABLE VIII. Temporal fitting ranges $t_{\min} \ldots t_{\max}$ and maximum topological charges $|Q|$ for the volumes V under consideration.

V	$t_{\min}$	$t_{\max}$	Maximum $|Q|$ for $1/(\chi_t V)$, $|Q|/(\chi_t V) < 1$	Maximum $|Q|$ for $1/(\chi_t V)$, $|Q|/(\chi_t V) < 0.5$
40^2	12	16	7	3
44^2	12	18	9	4
48^2	12	20	11	5
52^2	12	22	13	6
56^2	12	24	15	7
60^2	12	24	17	8

To determine the pion mass and the static potential from correlation functions evaluated in single topological sectors, $M_{\pi,|Q|}$ and $\mathcal{V}_{q\bar{q},|Q|}$, we follow the lines of Sec. V. We perform least-square fits using expansion (5.7) or (5.8) of the correlation functions. We choose a suitable fitting range $t_{\min} \ldots t_{\max}$, which typically leads to $\chi^2/\text{d.o.f.} \lesssim 1$. The stability of the resulting $M_{\pi,|Q|}$ and $\mathcal{V}_{q\bar{q},|Q|}$ has been checked by varying $t_{\min}$ and $t_{\max}$ by ± 1. The t ranges used for the determination of the pion mass are listed in Table VIII.

We perform fits in three different ways: (c) a single combined fit to all five observables [M_π, $\mathcal{V}_{q\bar{q}}(r = 1)$, $\mathcal{V}_{q\bar{q}}(r = 2)$, $\mathcal{V}_{q\bar{q}}(r = 3)$, $\mathcal{V}_{q\bar{q}}(r = 4)$]; (c$\mathcal{V}$) a single combined fit to the four static potential observables; and (s) five separate fits, one to each of the five observables. The results are collected in Table IX, along with reference values obtained in all sectors at $V = 60^2$.[14]

The conclusions are essentially the same as for Yang-Mills theory discussed in Sec. V. Results extracted indirectly, from simulations at fixed topology, are in agreement with those obtained directly. The magnitude of the errors is the same for the two expansions (5.7) and (5.8), and for the fitting methods c, c$\mathcal{V}$ and s. They are, however, larger by factors of ≈ 2 when we use the stringent constraint $1/(\chi_t V), |Q|/(\chi_t V) < 0.5$, since less input data are involved compared to $1/(\chi_t V), |Q|/(\chi_t V) < 1$. The fits all yield uncorrelated $\chi^2/\text{d.o.f.} \lesssim 1$, indicating that the fixed topology results are well described by both formulas (5.7) and (5.8).

For $|Q| = 0 \ldots 4$ and $V = 40^2 \ldots 60^2$, the $M_{\pi,|Q|,V}$ values are plotted in Fig. 12. Again we observe a strong dependence on the topological sector, in particular, in small volumes. From the expansion (5.7), $M_{\pi,|Q|,V}$ is expected to behave as approximation (2.4),

[14] In the continuum two-flavor Schwinger model, the pion mass is predicted as [45] $M_{\pi,\text{cont}} = 2.008\ldots \times (m_{\text{cont}}^2 g_{\text{cont}})^{1/3}$. Remarkably, there is almost perfect agreement with our result for M_π, if we insert the bare fermion mass and β given in Eq. (6.4), which yields $M_\pi \simeq 0.343$.

TABLE IX. Results for the pion mass M_π and the static potential $\mathcal{V}_{q\bar{q}}(r)$ at separations $r = 1, 2, 3, 4$, with and without topology fixing. In the column Method the equation number of the expansion is listed, c denotes one combined fit to all five observables, c$\mathcal{V}$ means one combined fit to the four static potential observables, and s indicates separate fits for each of the five observables.

Method	M_π	$\mathcal{V}_{q\bar{q}}(1)$	$\mathcal{V}_{q\bar{q}}(2)$	$\mathcal{V}_{q\bar{q}}(3)$	$\mathcal{V}_{q\bar{q}}(4)$
		All sectors, $V = 60^2$			
	0.3474(3)	0.1296(2)	0.2382(5)	0.3288(7)	0.4045(10)
	Fixed topology, $V \in \{40^2, 44^2, 48^2, 52^2, 56^2, 60^2\}$, $1/(\chi_t V)$, $\lvert Q\rvert/(\chi_t V) < 1$				
(5.7)c	0.3466(16)	0.1293(19)	0.2370(23)	0.3261(29)	0.4022(62)
(5.7)c$\mathcal{V}$		0.1295(10)	0.2372(12)	0.3386(15)	0.4052(16)
(5.7)s	0.3477(8)	0.1285(7)	0.2371(9)	0.3282(12)	0.4050(16)
(5.8)c	0.3467(10)	0.1293(6)	0.2377(9)	0.3321(32)	0.4059(69)
(5.8)c$\mathcal{V}$		0.1295(5)	0.2379(11)	0.3392(14)	0.4049(16)
(5.8)s	0.3477(9)	0.1294(5)	0.2374(6)	0.3288(12)	0.4040(15)
	Fixed topology, $V \in \{40^2, 44^2, 48^2, 52^2, 56^2, 60^2\}$, $1/(\chi_t V)$, $\lvert Q\rvert/(\chi_t V) < 0.5$				
(5.7)c	0.3454(32)	0.1284(27)	0.2364(28)	0.3311(50)	0.4049(80)
(5.7)c$\mathcal{V}$		0.1282(12)	0.2370(16)	0.3312(35)	0.4175(82)
(5.7)s	0.3478(32)	0.1292(12)	0.2377(21)	0.3275(61)	0.4027(91)
(5.8)c	0.3455(32)	0.1285(16)	0.2365(19)	0.3310(49)	0.4048(78)
(5.8)c$\mathcal{V}$		0.1287(9)	0.2371(23)	0.3312(36)	0.4073(83)
(5.8)s	0.3482(35)	0.1291(11)	0.2376(13)	0.3290(22)	0.4036(55)

$$M_{\pi,Q,V} = M_\pi + \frac{c}{V\chi_t}\left(1 - \frac{Q^2}{V\chi_t}\right),$$
$$c = \frac{1}{2}M''_\pi(\theta)_\pi|_{\theta=0}. \tag{6.8}$$

The corresponding curves for $|Q| = 0\ldots4$ with parameters M_π, M''_π and χ_t, determined by the previously discussed fit (5.7)s, are also shown in Fig. 12. One can clearly see that approximation (6.8) nicely captures the lattice results for $M_{\pi,|Q|,V}$.

We conclude, similar to our study in Yang-Mills theory, that it is possible to extract correct and accurate values for the pion mass and the static potential from correlation functions computed in a number of fixed topological sectors and volumes. The errors are somewhat larger than for direct computation, in our case by factors of $\approx 2\ldots7$. This is partly due to the smaller amount of gauge configurations of the fixed Q ensembles at different V, and partly due to the extrapolation to infinite volume.

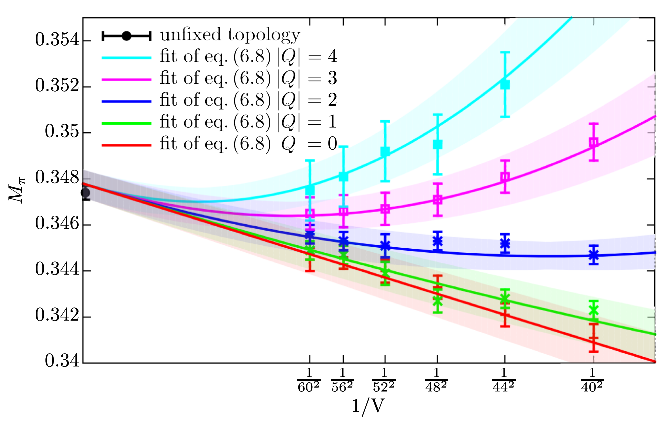

FIG. 12. The fixed topology pion mass $M_{\pi,|Q|,V}$ for $|Q| = 0\ldots4$, as a function of $1/V$, and the curves corresponding to formula (6.8).

2. The topological susceptibility

Table X presents results for the topological susceptibility extracted from our data for $M_{\pi,|Q|}$ and $\mathcal{V}_{q\bar{q},|Q|}$. These values for χ_t are obtained from the same fits, which lead to the results in Table IX. The results for χ_t and their interpretation are similar to those obtained in Yang-Mills theory. We observe a slight tension of $\approx 2\sigma$ for some values, when using expansion (5.7) and the relaxed constraint ($1/(\chi_t V)$, $|Q|/(\chi_t V) < 1$). This tension disappears when we apply the improved expansion (5.8). When imposing the strict constraint ($1/\chi_t V, |Q|/\chi_t V < 0.5$), we encounter the same problem as in Sec. V C 2: all results are in agreement with the directly measured $\chi_t = \langle Q^2\rangle/V$ (at $V = 60^2$), but the errors are very large.[15]

We infer that a reasonably accurate determination of the topological susceptibility from $M_{\pi,|Q|}$ and $\mathcal{V}_{q\bar{q},|Q|}$ requires extremely precise input data. The fixed topology ensembles and correlation functions of this work are not sufficient to extract an accurate and stable value for χ_t.

[15]Reference [46] presents results for χ_t in the two-flavor Schwinger model with staggered and overlap fermions, with or without link smearing. The results at $\beta = 4$ and $m = 0.1$ (in large volume) are in the range $\chi_t \simeq 0.044\ldots0.064$. This agrees with our value in Table X, which confirms the mild renormalization of our bare fermion mass (cf. footnote 14).

TABLE X. Results for the topological susceptibility χ_t, directly measured (at $V = 60^2$), and based on fixed topology computations of $M_{\pi,|Q|}$ and $\mathcal{V}_{q\bar{q},|Q|}(r)$ for separations $r = 1, 2, 3, 4$. In the column Method the equation number of the expansion is listed, c denotes a single combined fit to all five observables, c$\mathcal{V}$ means a single combined fit to the four static potential observables, and s denotes a separate fit to each of the five observables.

<table>
<tr><th>Method</th><th>M_π</th><th>$\mathcal{V}_{q\bar{q}}(1)$</th><th>$\mathcal{V}_{q\bar{q}}(2)$</th><th>$\mathcal{V}_{q\bar{q}}(3)$</th><th>$\mathcal{V}_{q\bar{q}}(4)$</th></tr>
<tr><td colspan="6">All sectors, $V = 60^2$</td></tr>
<tr><td></td><td colspan="5">0.0048(1)</td></tr>
<tr><td colspan="6">Fixed topology, $V \in \{40^2, 44^2, 48^2, 52^2, 56^2, 60^2\}$, $1/(\chi_t V)$, $|Q|/(\chi_t V) < 1$</td></tr>
<tr><td>(5.7)c</td><td colspan="5">0.0038(5)</td></tr>
<tr><td>(5.7)c$\mathcal{V}$</td><td></td><td colspan="4">0.0042(5)</td></tr>
<tr><td>(5.7)s</td><td>0.0041(4)</td><td>0.0038(5)</td><td>0.0036(7)</td><td>0.0038(11)</td><td>0.0044(9)</td></tr>
<tr><td>(5.8)c</td><td colspan="5">0.0044(4)</td></tr>
<tr><td>(5.8)c$\mathcal{V}$</td><td></td><td colspan="4">0.0042(6)</td></tr>
<tr><td>(5.8)s</td><td>0.0046(5)</td><td>0.0043(4)</td><td>0.0045(7)</td><td>0.0036(12)</td><td>0.0038(8)</td></tr>
<tr><td colspan="6">Fixed topology, $V \in \{40^2, 44^2, 48^2, 52^2, 56^2, 60^2\}$, $1/(\chi_t V)$, $|Q|/(\chi_t V) < 0.5$</td></tr>
<tr><td>(5.7)c</td><td colspan="5">0.0065(35)</td></tr>
<tr><td>(5.7)c$\mathcal{V}$</td><td></td><td colspan="4">0.0017(30)</td></tr>
<tr><td>(5.7)s</td><td>0.0014(38)</td><td>0.0049(32)</td><td>0.0057(31)</td><td>0.0037(48)</td><td>0.0032(27)</td></tr>
<tr><td>(5.8)c</td><td colspan="5">0.0067(32)</td></tr>
<tr><td>(5.8)c$\mathcal{V}$</td><td></td><td colspan="4">0.0018(33)</td></tr>
<tr><td>(5.8)s</td><td>0.0017(32)</td><td>0.0043(34)</td><td>0.0022(46)</td><td>0.0015(38)</td><td>0.0048(52)</td></tr>
</table>

VII. CONCLUSIONS

We have systematically explored the applicability of the BCNW method [14] with lattice data in fixed topological sectors. Our study encompasses the quantum rotor, the Heisenberg model, four-dimensional SU(2) Yang-Mills theory and the two-flavor Schwinger model. The originally suggested application to the pion mass has been extended to other observables, like the magnetic susceptibility and the static quark-antiquark potential.

The primary goal of this method is the determination of a physical observable if only fixed topology results are available. Our observations show that this can be achieved to a good precision with input data from various volumes and topological sectors, which obey the (rather relaxed) constraint $1/(\chi_t V), |Q|/(\chi_t V) < 1$. Hence this method is promising for application in QCD, where lattice spacings below $a \simeq 0.05$ fm are expected to confine HMC simulations to a single topological sector over extremely long trajectories.

As a second goal, this method also enables—in principle—the determination of the topological susceptibility χ_t. In our study we obtained the right magnitude also for χ_t, but the results were usually plagued by large uncertainties. For this purpose, i.e., for the measurement of χ_t based on fixed topology simulation results, other methods are more appropriate, based on the topological charge density correlation [21–23], or on an analysis of χ_t in subvolumes [24,26].

Regarding the optimal way to apply this method, it seems—for lattice data of typical statistical precision—not really helpful to add additional terms of the $1/(\chi_t V)$ expansion, beyond the incomplete second order that was suggested in Ref. [14]. Higher terms were elaborated in Ref. [16], and they improve the agreement with the fixed topology lattice data, but due to the appearance of additional free parameters they hardly improve the results for the physical observable and for χ_t.

A step beyond, which deserves being explored in more detail, is the inclusion of ordinary finite size effects (not related to topology fixing) [18], which even allows for the use of small volumes (in the terminology of Sec. II).

At this point, we recommend the application of the simple formulas (2.4) and (5.7) or (slightly better) (5.8), with only three free parameters, for the determination of hadron masses in QCD on fine lattices, in particular, in the presence of very light quarks.

ACKNOWLEDGMENTS

We thank Irais Bautista and Lilian Prado for their contributions to this project at an early stage, and Carsten Urbach for providing a simulation code for the Schwinger model, corresponding advice and helpful discussions. This work was supported by the Helmholtz International Center for FAIR within the framework of the LOEWE program launched by the State of Hesse, and by the Mexican Consejo Nacional de Ciencia y Tecnología (CONACYT) through Grants No. CB-2010/155905 and No. CB-2013/222812, as well as DGAPA-UNAM, Grant No. IN107915. A. D., C. C. and M. W. acknowledge support by the Emmy Noether Program of the German Research Foundation (DFG), Grant No. WA 3000/1-1, and C. P. H. was supported through the project Redes Temáticas de Colaboración Académica 2013, Grant No. UCOL-CA-56. Calculations were performed on the LOEWE-CSC and

FUCHS-CSC high-performance computer of Frankfurt University, and on the cluster of ICN/UNAM. We also thank HPC-Hessen, funded by the State Ministry of Higher Education, Research and the Arts, for programing advice.

APPENDIX: LOW TEMPERATURE EXPANSION OF THE MAGNETIC SUSCEPTIBILITY OF THE QUANTUM ROTOR

Our point of departure is Eq. (3.10) for the magnetic susceptibility of the quantum rotor at fixed topology,[16]

$$\chi_{\mathrm{m},Q} = \int_0^{L/2} dt\ e^{(t^2/L-t)/(2\beta)}[e^{2\pi \mathrm{i}Qt/L} + e^{-2\pi \mathrm{i}Qt/L}]. \tag{A1}$$

By completing the squares in each term, and defining

$$z_0 = \sqrt{\frac{L}{8\beta}}\left(1+\frac{4\pi \mathrm{i}Q\beta}{L}\right), \tag{A2}$$

we obtain

$$\begin{aligned}\chi_{\mathrm{m},Q} &= \sqrt{2\beta L}e^{\frac{2\pi^2\beta Q^2}{L}-\frac{L}{8\beta}}(-1)^Q\left[\int_{-z_0}^{-\pi \mathrm{i}Q\sqrt{2\beta/L}} dt\ e^{t^2} + \int_{-z_0^*}^{\pi \mathrm{i}Q\sqrt{2\beta/L}} dt\ e^{t^2}\right] \\ &= \sqrt{\frac{\pi\beta L}{2}}e^{\frac{2\pi^2\beta Q^2}{L}-\frac{L}{8\beta}}(-1)^Q[\mathrm{erfi}(z_0)+\mathrm{erfi}(z_0^*)] \\ &= \sqrt{8\beta L}\,\mathrm{Re}D(z_0).\end{aligned} \tag{A3}$$

[16] Since this entire appendix refers to continuous Euclidean time, we skip for simplicity the subscripts of β_{cont} and L_{cont}.

We have used two properties of the imaginary error function, $\mathrm{erfi}(z) = -\mathrm{erfi}(-z)$ and $\mathrm{erfi}(z^*) = (\mathrm{erfi}(z))^*$, and in the last step we inserted Dawson's function,

$$D(z) = \frac{\sqrt{\pi}}{2}e^{-z^2}\mathrm{erfi}(z) = e^{-z^2}\int_0^z dt\ e^{t^2}. \tag{A4}$$

We are interested in the case $L \gg \beta$ where $|\arg(\mathrm{i}z_0)| \approx \frac{\pi}{2} < \frac{3\pi}{4}$, so we can apply the asymptotic expansion [47],

$$\begin{aligned}D(z_0) &= \frac{1}{2z_0}\sum_{n\geq 0}\frac{(2n-1)!!}{(2z_0^2)^n} \\ &= \frac{1}{2z_0}\left(1+\frac{1}{2z_0^2}+\frac{3}{4z_0^4}+\frac{15}{8z_0^6}+\mathcal{O}(|z_0|^{-8})\right).\end{aligned} \tag{A5}$$

If we expand

$$\chi_{\mathrm{m},Q} \simeq 4\beta\mathrm{Re}\left[\frac{1}{1+4\pi \mathrm{i}Q\beta/L}\left(1+\frac{1}{2z_0^2}+\frac{3}{4z_0^4}+\frac{15}{8z_0^6}\right)\right] \tag{A6}$$

to $\mathcal{O}((\beta/L)^3)$, and insert the infinite volume limit $\chi_{\mathrm{m}} = 4\beta$, we arrive at

$$\begin{aligned}\chi_{\mathrm{m},Q} = \chi_{\mathrm{m}} + \beta\Bigg[&\frac{16\beta}{L}+\frac{64\beta^2}{L^2}(3-(\pi Q)^2) \\ &+\frac{768\beta^3}{L^3}(5-2(\pi Q)^2)+\mathcal{O}\left(\left(\frac{\beta}{L}\right)^4\right)\Bigg].\end{aligned} \tag{A7}$$

By substituting $\chi_{\mathrm{t}} = \frac{1}{4\pi^2\beta}$ (which only has exponentially suppressed finite size effects [26]), we confirm to each order given in Eq. (A7) the expansion that we anticipated in Eq. (3.11); it is not altered by the truncation of the Gauss integrals.

[1] P. Hasenfratz, V. Laliena, and F. Niedermayer, The index theorem in QCD with a finite cutoff, Phys. Lett. B **427**, 125 (1998).
[2] B. Berg and M. Lüscher, Definition and statistical distributions of a topological number in the lattice O(3) sigma model, Nucl. Phys. **B190**, 412 (1981).
[3] P. de Forcrand, M. García Pérez, and I.-O. Stamatescu, Topology of the SU(2) vacuum: a lattice study using improved cooling, Nucl. Phys. **B499**, 409 (1997).
[4] F. Bruckmann, F. Gruber, K. Jansen, M. Marinkovic, C. Urbach, and M. Wagner, Comparing topological charge definitions using topology fixing actions, Eur. Phys. J. A **43**, 303 (2010).
[5] K. Cichy, E. Garcia-Ramos, and K. Jansen, Topological susceptibility from the twisted mass Dirac operator spectrum, J. High Energy Phys. 02 (2014) 119.
[6] K. Cichy, A. Dromard, E. Garcia-Ramos, K. Ottnad, C. Urbach, M. Wagner, U. Wenger, and F. Zimmermann, Comparison of different lattice definitions of the topological charge, *Proc. Sci.*, LATTICE2014, 075 [arXiv:1411.1205].
[7] H. Fukaya *et al.*, Two-Flavor Lattice QCD Simulation in the Epsilon Regime with Exact Chiral Symmetry, Phys. Rev. Lett. **98**, 172001 (2007); H. Fukaya, S. Aoki, T. W. Chiu, S. Hashimoto, T. Kaneko, H. Matsufuru, J. Noaki, K. Ogawa, T. Onogi, and N. Yamada, Two-flavor lattice QCD in the ϵ regime and chiral random matrix theory, Phys. Rev. D **76**,

054503 (2007); S. Aoki *et al.* (JLQCD Collaboration), Two-flavor QCD simulation with exact chiral symmetry, Phys. Rev. D **78**, 014508 (2008); Sz. Borsanyi *et al.*, QCD thermodynamics with continuum extrapolated dynamical overlap fermions, arXiv:1510.03376.

[8] G. I. Egri, Z. Fodor, S. D. Katz, and K. K. Szabo, Topology with dynamical overlap fermions, J. High Energy Phys. 01 (2006) 049.

[9] H. Fukaya, S. Hashimoto, T. Hirohashi, K. Ogawa, and T. Onogi, Topology conserving gauge action and the overlap-Dirac operator, Phys. Rev. D **73**, 014503 (2006); W. Bietenholz, K. Jansen, K.-I. Nagai, S. Necco, L. Scorzato, and S. Shcheredin, Exploring topology conserving gauge actions for lattice QCD, J. High Energy Phys. 03 (2006), 017.

[10] D. Banerjee, M. Bögli, K. Holland, F. Niedermayer, M. Pepe, U. Wenger, and U.-J. Wiese, An improved single-plaquette gauge action, J. High Energy Phys. 03 (2016) 116.

[11] K. Cichy, G. Herdoiza, and K. Jansen, Continuum limit of overlap valence quarks on a twisted mass sea, Nucl. Phys. **B847**, 179 (2011); K. Cichy, V. Drach, E. Garcia-Ramos, G. Herdoiza, and K. Jansen, Overlap valence quarks on a twisted mass sea: a case study for mixed action lattice QCD, Nucl. Phys. **B869**, 131 (2013).

[12] M. Lüscher, Properties and uses of the Wilson flow in lattice QCD, J. High Energy Phys. 08 (2010) 071; Topology, the Wilson flow and the HMC algorithm, *Proc. Sci.*, LATTICE2010, 015 [arXiv:1009.5877]; M. Lüscher and S. Schaefer, Lattice QCD without topology barriers, J. High Energy Phys. 07 (2011) 036; G. McGlynn and R. D. Mawhinney, Diffusion of topological charge in lattice QCD simulations, Phys. Rev. D **90**, 074502 (2014).

[13] S. Mages, B. C. Tóth, S. Borsányi, Z. Fodor, S. Katz, and K. K. Szabó, Lattice QCD on nonorientable manifolds, arXiv:1512.06804.

[14] R. Brower, S. Chandrasekharan, J. W. Negele, and U.-J. Wiese, Physical observables from lattice QCD at fixed topology, Nucl. Phys. B, Proc. Suppl. **106**, 581 (2002); QCD at fixed topology, Phys. Lett. B **560**, 64 (2003).

[15] A. Dromard and M. Wagner, Studying and removing effects of fixed topology in a quantum mechanical model, *Proc. Sci.*, LATTICE2013, 339 [arXiv:1309.2483].

[16] A. Dromard and M. Wagner, Extracting hadron masses from fixed topology simulations, Phys. Rev. D **90**, 074505 (2014).

[17] C. Czaban, A. Dromard, and M. Wagner, Studying and removing effects of fixed topology, Acta Phys. Pol. **7**, 551 (2014).

[18] A. Dromard, W. Bietenholz, U. Gerber, H. Mejía-Díaz, and M. Wagner, Simulations at fixed topology: Fixed topology versus ordinary finite volume corrections, Acta Phys. Pol. **8**, 391 (2015); Combining ordinary and topological finite volume effects for fixed topology simulations, arXiv:1510.08809.

[19] W. Bietenholz, I. Hip, S. Shcheredin, and J. Volkholz, A numerical study of the two-flavor Schwinger model with dynamical overlap hypercube fermions, Eur. Phys. J. C **72**, 1938 (2012).

[20] W. Bietenholz and I. Hip, Topological summation of observables measured with dynamical overlap fermions, *Proc. Sci.*, LATTICE2008, 079 [arXiv:0808.3049]; Topological summation in lattice gauge theory, J. Phys. Conf. Ser. **378**, 012041 (2012).

[21] S. Aoki, H. Fukaya, S. Hashimoto, and T. Onogi, Finite volume QCD at fixed topological charge, Phys. Rev. D **76**, 054508 (2007).

[22] I. Bautista, W. Bietenholz, A. Dromard, U. Gerber, C. P. Hofmann, H. Mejía-Díaz, and M. Wagner, Measuring the topological susceptibility in a fixed sector, Phys. Rev. D **92**, 114510 (2015).

[23] S. Aoki *et al.* (JLQCD and TWQCD Collaborations), Topological susceptibility in two-flavor lattice QCD with exact chiral symmetry, Phys. Lett. B **665**, 294 (2008); Topology density correlator on dynamical domain-wall ensembles with nearly frozen topological charge, *Proc. Sci.*, LATTICE2014, 323 [arXiv:1411.1473].

[24] R. C. Brower *et al.* (LSD Collaboration), Maximum-likelihood approach to topological charge fluctuations in lattice gauge theory, Phys. Rev. D **90**, 014503 (2014).

[25] A. Laio, G. Martinelli, and F. Sanfilippo, Metadynamics surfing on topology barriers: the $CP(\mathrm{N}-1)$ case, arXiv:1508.07270.

[26] W. Bietenholz, P. de Forcrand, and U. Gerber, Topological susceptibility from slabs, J. High Energy Phys. 12 (2015) 070.

[27] C. Czaban and M. Wagner, Lattice study of the Schwinger model at fixed topology, *Proc. Sci.*, LATTICE2013, 465 [arXiv:1310.5258]; I. Bautista, W. Bietenholz, U. Gerber, C. P. Hofmann, H. Mejía-Díaz, and L. Prado, Interpretation of topologically restricted measurements in lattice sigma models, arXiv:1402.2668; U. Gerber, I. Bautista, W. Bietenholz, H. Mejía-Díaz, and C. P. Hofmann, Extracting physics from topologically frozen Markov chains, *Proc. Sci.*, LATTICE2014, 320 [arXiv:1410.0426]; A. Dromard, C. Czaban, and M. Wagner, Hadron masses from fixed topology simulations: Parity partners and SU(2) Yang-Mills results, *Proc. Sci.*, LATTICE2014, 321 [arXiv:1410.4333].

[28] W. Bietenholz, R. Brower, S. Chandrasekharan, and U.-J. Wiese, Perfect lattice topology: The quantum rotor as a test case, Phys. Lett. B **407**, 283 (1997).

[29] L. S. Schulman, *Techniques and Applications of Path Integration* (John Wiley & Sons, New York, 1981).

[30] N. Manton, An alternative action for lattice gauge theories, Phys. Lett. **96B**, 328 (1980).

[31] U. Wolff, Collective Monte Carlo Updating for Spin Systems, Phys. Rev. Lett. **62**, 361 (1989).

[32] W. Bietenholz, U. Gerber, M. Pepe, and U.-J. Wiese, Topological lattice actions, J. High Energy Phys. 12 (2010) 020.

[33] L. Del Debbio, H. Panagopoulos, and E. Vicari, Theta dependence of SU(N) gauge theories, J. High Energy Phys. 08 (2002) 044.

[34] S. Schaefer, R. Sommer, and F. Virotta (ALPHA Collaboration), Critical slowing down and error analysis in lattice QCD simulations, Nucl. Phys. **B845**, 93 (2011).

[35] M. Creutz, *Quarks, Gluons, and Lattices* (Cambridge University Press, Cambridge, 1983).

[36] O. Philipsen and M. Wagner, On the definition and interpretation of a static quark-antiquark potential in the color-adjoint channel, Phys. Rev. D **89**, 014509 (2014).

[37] M. Albanese *et al.* (APE Collaboration), Glueball masses and string tension in lattice QCD, Phys. Lett. B **192**, 163 (1987).

[38] A. Hasenfratz and F. Knechtli, Flavor symmetry and the static potential with hypercubic blocking, Phys. Rev. D **64**, 034504 (2001); M. Della Morte, S. Dürr, J. Heitger, H. Molke, J. Rolf, A. Shindler, and R. Sommer (ALPHA Collaboration), Lattice HQET with exponentially improved statistical precision, Phys. Lett. B **581**, 93 (2004); Erratum to: Lattice HQET with exponentially improved statistical precision, Phys. Lett. B **612**, 313 (2005); M. Della Morte, A. Shindler, and R. Sommer, On lattice actions for static quarks, J. High Energy Phys. 08 (2005) 051.

[39] K. Jansen, C. Michael, A. Shindler, and M. Wagner (ETM Collaboration), The static-light meson spectrum from twisted mass lattice QCD, J. High Energy Phys. 12 (2008) 058.

[40] H. J. Rothe, *Lattice Gauge Theories: An Introduction* (World Scientific, Singapore, 2005).

[41] M. Lüscher, Topology of lattice gauge fields, Commun. Math. Phys. **85**, 39 (1982); C. R. Gattringer, I. Hip, and C. B. Lang, Topological charge and the spectrum of the fermion matrix in lattice QED in two dimensions, Nucl. Phys. **B508**, 329 (1997).

[42] C. Urbach, https://github.com/urbach/schwinger.

[43] M. Hasenbusch, Speeding up the hybrid Monte Carlo algorithm for dynamical fermions, Phys. Lett. B **519**, 177 (2001).

[44] M. Wagner, S. Diehl, T. Kuske, and J. Weber, An introduction to lattice hadron spectroscopy for students without quantum field theoretical background, arXiv:1310.1760.

[45] A. V. Smilga, Critical amplitudes in two-dimensional theories, Phys. Rev. D **55**, R443(R) (1997).

[46] S. Dürr and C. Hoelbling, Staggered versus overlap fermions: A study in the Schwinger model with $\mathrm{N(f)} = 0, 1, 2$, Phys. Rev. D **69**, 034503 (2004).

[47] M. Abramowitz and I. A. Stegun, *Handbook of Mathematical Functions* (Dover Publications, New York, 1972).